

Calculating spin-lattice interactions in ferro- and antiferromagnets: the role of symmetry, dimension and frustration

Hannah Lange,¹ Sergiy Mankovsky,¹ Svitlana Polesya,¹ Markus Weißenhofer,² Ulrich Nowak,² and Hubert Ebert¹

¹*Department of Chemistry/Phys. Chemistry, LMU Munich,
Butenandtstrasse 11, D-81377 Munich, Germany*

²*Department of Physics, University of Konstanz, DE-78457 Konstanz, Germany*

(Dated: March 17, 2023)

Recently, the interplay between spin and lattice degrees of freedom has gained a lot of attention due to its importance for various fundamental phenomena as well as for spintronic and magnonic applications. Examples are ultrafast angular momentum transfer between the spin and lattice subsystems during ultrafast demagnetization, frustration driven by structural distortions in transition metal oxides, or in acoustically driven spin-wave resonances. In this work, we provide a systematic analysis of spin-lattice interactions for ferro- and antiferromagnetic materials and focus on the role of lattice symmetries and dimensions, magnetic order, and the relevance of spin-lattice interactions for angular momentum transfer as well as magnetic frustration. For this purpose, we use a recently developed scheme which allows an efficient calculation of spin-lattice interaction tensors from first principles. In addition to that, we provide a more accurate and self consistent scheme to calculate ab initio spin lattice interactions by using embedded clusters which allows to benchmark the performance of the scheme introduced previously.

I. INTRODUCTION

The interplay of the magnetic and lattice degrees of freedom is crucial for a number of phenomena observed for magnetic materials. Consequently, the investigation of spin-lattice interactions is of great importance as it gives access to the understanding of a variety of phenomena observed in magnetic materials, as for instance frustration driven structural distortions in different transition metal oxides [1–3] and dichalcogenides [4, 5], or mutual modifications of the magnon and phonon spectra in the magnetically ordered state [6–9]. Such a modification of the phonon spectra can be seen for example by making use of Raman spectroscopy. This was indeed demonstrated for multilayered CrI₃, for which the modification of the Raman spectrum is associated with the corresponding change of the phonon modes induced by manipulating the interlayer alignment of magnetic moments in the presence of a magnetic field [10]. In addition, a significant role of the the Dzyaloshinskii-Moriya interactions (DMI) in this material even without taking into account lattice vibrations has been demonstrated theoretically, with a strong impact of the DMI on the magnon spectrum [11, 12]. Moreover, a crucial role of pronounced DMI-like spin-lattice interactions for the existence of topological magnons was also discussed on the basis of first-principles calculations in Ref. [13]. Interestingly, this phenomenon may be used for ultrafast optical control of magnetism as discussed in the literature [14, 15]. Furthermore, recent experimental and theoretical works show that spin-lattice interactions play a crucial role for the angular momentum transfer during ultrafast demagnetization [16, 17]. Apart from that, spin-lattice coupling has attracted increasingly attention during last decade in view of its potential exploitation in spintronics and magnonics, seen as a way to control magnetic properties. This can be

done for example by means of acoustic wave excitations, or via the application of external mechanical forces. In particular, spin-lattice interactions can be used for the control of the domain wall motion by optically generated magnetoelastic waves [18], for spin current generation by surface acoustic waves in ferromagnetic layers via magnon-phonon coupling (inverse Edelstein effect [19]), or for the control of the spin wave resonance frequency by means of surface acoustic waves [20].

In this context the need for reliable schemes to investigate spin-lattice interactions as well as their dependence on the material under consideration emerges [21–24]. This field of research is only at its beginning and to our knowledge no systematic investigation of the role of spin-lattice coupling for a series of materials has been done yet. A promising way to gain insight in spin-lattice phenomena are atomistic simulations that simultaneously model the time evolution of both spin and lattice degrees of freedom [25–28]. This approach obviously requires a corresponding extension of the underlying model Hamiltonian to account for the coupling between them [29–31]. Accordingly, in order to perform such simulations, besides spin-spin exchange coupling (SSC) tensors also spin-lattice exchange coupling (SLC) tensors are needed as an input. Recent works have provided first schemes to calculate these tensors based on supercell and perturbative SLC approaches [13, 30, 31].

In this work, an accurate and efficient method based on embedded cluster calculations is presented and compared to the existing schemes. Furthermore, we calculate the SLC tensors for ferro- and antiferromagnetic materials with different magnetic order, lattice structure and dimensionality using the Korringa-Kohn-Rostoker (KKR) Green function method [32] and systematically investigate the symmetry of the SLC tensors w.r.t. the crystal symmetry as well as the physical relevance of SLC to angular momentum transfer and magnetoelastic transitions

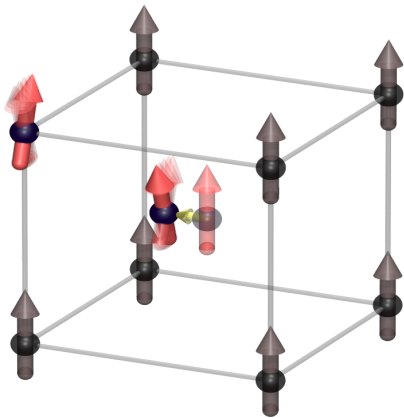


Figure 1. Geometry for the calculation of the spin-lattice exchange coupling using the embedded cluster method (here for $i = k$).

in frustrated antiferromagnets like metal-dichalcogenides and -oxides.

To describe the coupling of spin and spatial degrees of freedom we adopt the atomistic spin-lattice Hamiltonian as proposed by Hellsvik et al. [30] and Mankovsky et al. [31], i.e.

$$\mathcal{H}_{sl} = - \sum_{i,j,\alpha,\beta} J_{ij}^{\alpha\beta} e_i^\alpha e_j^\beta - \sum_{i,j,\alpha,\beta} \sum_{k,\mu} \mathcal{J}_{ij,k}^{\alpha\beta,\mu} e_i^\alpha e_j^\beta u_k^\mu + \dots (1)$$

with the spin-orientation vectors e_i , atomic displacement vectors \mathbf{u}_k , spin-spin coupling (SSC) tensor elements $J_{ij}^{\alpha\beta}$ and spin-lattice coupling (SLC) tensor elements $J_{ij,k}^{\alpha\beta,\mu} = \frac{\partial J_{ij}^{\alpha\beta}}{\partial u_k^\mu}$. Eq. (1) can be extended further to spin-lattice interactions of any order. Note that we focus on magnetic interactions and hence omit pure lattice terms in Eq. (1) that involve real space force constants.

It should be mentioned that the mutual influence of spin and lattice dynamical properties have already been investigated previously using various approaches. A prominent example for this is the consideration of local spin-phonon interactions induced by a crystal field modulated due to a local lattice distortion [33–35]. Another approach based on ab-initio total energy calculations treats the coupling parameters as fitting parameters [29, 36] as done within the often used *Conolly-Williams* approach [37]. In this case, ab-initio electronic structure calculations have to be performed for a set of configurations large enough to fix all parameters for the chosen form of the Hamiltonian. Including the lattice in addition to the spin degrees of freedom obviously will make the fitting procedure much more demanding than considering a plain spin Hamiltonian.

On the other hand, the so-called Lichtenstein formula [38] is a well established approach for ab initio calculations of the isotropic spin-spin coupling parameters, with extensions to account for the full tensorial form

of the interaction parameters [39, 40] and a multi-site expansion [41]. In contrast, the calculation of spin-lattice interaction parameters has received interest only recently. Refs. [13, 30] have suggested to calculate the corresponding spin-lattice exchange coupling parameters from first principles by using supercells and calculating the SLC as the modification of the SSC when displacing an atom in each supercell. This method becomes accurate for sufficiently large supercells but is restricted to a small number of interacting atoms and relatively small supercells due to its high computational costs. Recently, Mankovsky et al. [31] have derived closed expressions to calculate the spin-lattice coupling tensors in a fully-relativistic way by treating the modifications in spin and lattice configurations on the same, perturbative level. It was shown that this method enables the calculation of fully relativistic SLC tensors which are in satisfying agreement with SLC tensors obtained by the supercell method.

The present paper is organized as follows: In the first two sections, we briefly review the spin-lattice coupling methods presented in Ref. [31], i.e. the supercell and perturbative method, and compare the results for bcc Fe to a new method based on embedded clusters, which enables a more efficient and accurate calculation of the SLC than the supercell method. Consequently we consider it as a more appropriate method to benchmark the perturbative SLC method presented in Ref. [31], enabling a robust way of calculating spin-lattice interactions up to any order of displacements and spin tiltings. Comparing these results for all methods we find good agreement, which allows us to use the perturbative SLC method to systematically investigate spin-lattice coupling. In a first step, we consider the symmetry of the SLC tensors w.r.t. the crystal structure of the considered material and find that the symmetry of the lattice (in combination with spin-orbit coupling) gives rise to specific non-vanishing SLC contributions, e.g. Dzyaloshinskii–Moriya like interactions. In a second step, we calculate the SLC tensors for various materials with different lattice configurations and magnetic structures and consider the role of the dimensionality by calculating the SLC for free standing monolayers and 2D deposited magnetic films. Lastly, we investigate the SLC contribution to magnetoelastic transitions in frustrated antiferromagnets.

II. THEORETICAL BACKGROUND

The field of spin-lattice coupling is still at its beginning. The first ones to calculate *ab initio* spin-lattice interaction parameters for the non-relativistic case were Hellsvik et al. [30], who suggested to calculate the elements of the corresponding spin-lattice exchange coupling tensor from the modification of the spin-spin exchange coupling $J_{ij}^{\alpha\beta}(\mathbf{u}_k)$ due to a displacement u_k^μ . Focusing here on the spin-lattice interaction term in the

Hamiltonian, $\frac{\partial}{\partial u_k^\mu} J_{ij}^{\alpha\beta}(\mathbf{u}_k) u_k^\mu$, linear with respect to displacement u_k^μ , the corresponding coupling parameters $J_{ij,k}^{\alpha\beta,\mu}$ can be delivered by calculating the derivative of $J_{ij}^{\alpha\beta}(\mathbf{u}_k)$ numerically as follows

$$J_{ij,k}^{\alpha\beta,\mu} = \frac{\partial}{\partial u_k^\mu} J_{ij}^{\alpha\beta}(\mathbf{u}_k) \approx \frac{J_{ij}^{\alpha\beta}(u_k^\mu) - J_{ij}^{\alpha\beta}(0)}{u_k^\mu} \quad (2)$$

considering the displacement u_k^μ in the limit of $u_k^\mu \rightarrow 0$.

As suggested by Hellsvik et al. [30], the ordinary exchange coupling parameters $J_{ij}^{\alpha\beta}(\mathbf{u}_k)$ can be calculated by making use of a scheme introduced by Liechtenstein and coworkers leading to the so-called Liechtenstein or LKAG formula [38]. This approach that makes use of the magnetic force theorem implies the evaluation of the free energy change due to a perturbation of the system, which can be written within the multiple-scattering formalism [32] as follows

$$\Delta\mathcal{F} = -\frac{1}{\pi} \text{Im} \text{Tr} \int^{E_F} dE (\ln \underline{\tau}(E) - \ln \underline{\tau}^0(E)) , \quad (3)$$

with the scattering path operator of the unperturbed reference system

$$\underline{\tau}^{(0)}(E) = \left[\underline{\underline{m}}^{(0)}(E) - \underline{\underline{G}}(E) \right]^{-1} , \quad (4)$$

and of the perturbed system

$$\underline{\tau}(E) = \left[\underline{\underline{m}}(E) - \underline{\underline{G}}(E) \right]^{-1} , \quad (5)$$

with $\underline{\underline{G}}(E)$ the structural Green function and $\underline{\underline{m}}^{(0)}(E) = [\underline{t}^{(0)}(E)]^{-1}$ the inverse of the site-diagonal single-site scattering matrix $\underline{t}^{(0)}(E)$, and double underlines indicating matrices with respect to site and spin-angular momentum indices.

According to the LKAG scheme, the expression for the exchange coupling parameter J_{ij} is derived accounting for the perturbations due to a spin tilting $\delta\hat{e}_{i(j)}^\alpha$ on sites i and j . As this perturbation leads to a corresponding change of the inversed single-site scattering matrix $\Delta_\alpha^s \underline{m}_i = \underline{m}_i(\delta\hat{e}_i^\alpha) - \underline{m}_i^0$, the change of the free energy in Eq. (3) can be evaluated using the expression

$$\ln \underline{\tau} - \ln \underline{\tau}^0 = -\ln \left(1 + \underline{\tau} [\Delta_\alpha^s \underline{m}_i + \Delta_\beta^s \underline{m}_j + \dots] \right) . \quad (6)$$

With the change of the inversed single-site scattering matrix represented in terms of so-called torque operator \underline{T}_i^μ by the expression

$$\Delta_\mu^s \underline{m}_i = \delta\hat{e}_i^\alpha \underline{T}_i^\alpha , \quad (7)$$

linear with respect to spin tilting, one obtains a direct access to the exchange coupling parameters determined as the free energy derivative $\frac{\partial^2 \mathcal{F}}{\partial e_i^\alpha \partial e_j^\beta}$ [42]:

$$J_{ij}^{\alpha\beta} = -\frac{1}{\pi} \Im \text{Tr} \int dE \underline{T}_i^\alpha \underline{\tau}^{ij} \underline{T}_i^\beta \underline{\tau}^{ji} . \quad (8)$$

To get access to the full exchange coupling tensor Eq. (8) has to be evaluated within a fully relativistic framework [39, 40] with the multiple-scattering representation for the electronic Green function $G(\mathbf{r}, \mathbf{r}', E)$ in real space, given by the expression [43]

$$\begin{aligned} G(\mathbf{r}, \mathbf{r}', E) = & \sum_{\Lambda_1 \Lambda_2} Z_{\Lambda_1}^i(\mathbf{r}, E) \tau_{\Lambda_1 \Lambda_2}^{ij}(E) Z_{\Lambda_2}^{j \times}(\mathbf{r}', E) \\ & - \sum_{\Lambda_1} \left[Z_{\Lambda_1}^i(\mathbf{r}, E) J_{\Lambda_1}^{i \times}(\mathbf{r}', E) \Theta(r' - r) \right. \\ & \left. J_{\Lambda_1}^i(\mathbf{r}, E) Z_{\Lambda_1}^{i \times}(\mathbf{r}', E) \Theta(r - r') \right] \delta_{ij} , \quad (9) \end{aligned}$$

with the four-component wave functions $Z_\Lambda^n(\mathbf{r}, E)$ ($J_\Lambda^n(\mathbf{r}, E)$) are regular (irregular) solutions to the single-site Dirac equation [44, 45]. The elements of the matrix \underline{T}_i^μ in Eq. (7) are given by the expression

$$T_{i, \Lambda \Lambda'}^\alpha = \int_{\Omega_i} d^3r Z_\Lambda^{i \times}(\mathbf{r}, E) \left[\beta \sigma_\alpha B_{xc}^i(\mathbf{r}) \right] Z_{\Lambda'}^i(\mathbf{r}, E) \quad (10)$$

with $B_{xc}^i(\mathbf{r})$ being the spin-dependent part of the exchange-correlation potential, σ_α the Pauli matrix and β the standard Dirac matrix [46].

A. Super cell approach

As demonstrated by Hellsvik et al. [30] and Mankovsky et al. [31], Eq. (8) can be used straightforwardly to calculate the exchange coupling parameter $J_{ij}^{\alpha\beta}(\mathbf{u}_k)$ in the presence of an atomic displacement on site k . Such calculations can be easily done also on the basis of the recently reported approach based on Green's functions constructed using Wannier functions as a local basis set [47], that gives access to an alternative way for the calculation of SLC parameters. When performing these calculations using the multiple scattering formalism the scattering path operator $\underline{\tau}(\mathbf{u}_k)$ is determined selfconsistently for a supercell, big enough to minimize the impact on the exchange coupling tensor J_{ij} of the displacement periodically repeated in the neighboring cells. Note that selfconsistent calculations have a crucial impact on the accuracy of the results, as in this case a relaxation of the charge density around a displaced atom is taken into account. On the other hand, an important disadvantage of supercell calculations is their computational cost in the case of larger cells, or the other way around, they lead to the increasing inaccuracy when the supercell size is too small.

B. Embedded cluster approach

The disadvantages of the super cell approach – high numerical costs and a possible influence of neighboring super cells – can be avoided by making use of the Dyson equation for the Green function

$$\mathcal{G} = \mathcal{G}_0 + \mathcal{G}_0 \Delta V \mathcal{G} \quad (11)$$

where \mathcal{G}_0 is the Green function of a suitable reference system, while \mathcal{G} accounts for the perturbation $\Delta\mathcal{V}$.

To get access to the exchange parameter $J_{ij}^{\alpha\beta}(\mathbf{u}_k)$ between site i and j for site k displaced by \mathbf{u}_k one considers an atomic cluster centered on site k and big enough to include all sites i and j of interest. In a first step the Green function \mathcal{G} for this embedded cluster is calculated self-consistently using Eq. (11) with $\Delta\mathcal{V}$ accounting for the displacement of site k and its range given by the size of the embedded cluster. Using the real space representation $G(\mathbf{r}, \mathbf{r}', E)$ of the electronic Green function given by Eq. (9) allows to replace the Dyson equation (11) by the corresponding equivalent matrix equation for the scattering path operators [32]:

$$\underline{\underline{\tau}}_k(E) = [(\underline{\underline{t}}_k(E))^{-1} - (\underline{\underline{t}}_0(E))^{-1} - (\underline{\underline{\tau}}_0(E))^{-1}]^{-1}. \quad (12)$$

Here the second underline indicates matrices w.r.t. to the site indices numbering the sites within the cluster. Accordingly, the scattering path operator matrices $\underline{\underline{\tau}}_0(E)$ and $\underline{\underline{\tau}}_k(E)$ represent the unperturbed system in the regime of the cluster and the embedded cluster with atom k displaced by \mathbf{u}_k , respectively. Finally, the single site matrices $\underline{\underline{t}}_0(E)$ and $\underline{\underline{t}}_k(E)$ are site diagonal and represent the cluster atoms in case of the unperturbed system and the embedded cluster, respectively.

Having solved the embedding problem charge self-consistently the exchange coupling parameter $J_{ij}^{\alpha\beta}(\mathbf{u}_k)$ can be obtained from Eq. (8) using the corresponding blocks $\underline{\underline{\tau}}^{ij}(E)$ and $\underline{\underline{\tau}}^{ji}(E)$ of the super matrix $\underline{\underline{\tau}}_k(E)$.

C. Perturbative approach

Mankovsky et al. [31] suggested a perturbative scheme to get direct acces to the SLC parameter $J_{ij}^{\alpha\beta,\mu}$ without the numerical differentiation indicated by Eq. (2) and to avoid this way high numerical effort and any spurious inter-cell effects. The central idea is to extend the scheme underlying the Lichtenstein formula by accounting simultaneously for the impact of a distorted spin configuration $\{\delta\hat{e}_i\}$ and of atomic displacements $\{\mathbf{u}_k\}$. As a result, the change in the free energy w.r.t. an unperturbed reference state is given in terms of the scattering path operator the expression

$$\ln \underline{\underline{\tau}} - \ln \underline{\underline{\tau}}^0 = -\ln \left(1 + \underline{\underline{\tau}} [\Delta_\alpha^s \underline{\underline{m}}_i + \Delta_\beta^s \underline{\underline{m}}_j + \Delta_\mu^u \underline{\underline{m}}_k + \dots] \right) \quad (13)$$

where $\Delta_\mu^u \underline{\underline{m}}_k = \underline{\underline{m}}_k(u_k^\mu) - \underline{\underline{m}}_k^0$ is a change of the inverse single-site scattering matrix due to atomic displacement on site k . A linear approximation applied to $\Delta_\mu^u \underline{\underline{m}}_k$ representing it in terms of the so-called displacement operator \mathcal{U}_k^μ [48, 49] by the expression

$$\Delta_\mu^u \underline{\underline{m}}_k = u_k^\mu \mathcal{U}_k^\mu \quad (14)$$

allows us to work out explicit expression for the SLC parameters $J_{ij}^{\alpha\beta,\mu}$ as

$$J_{ij,k}^{\alpha\beta,\mu} = -\frac{\partial^3 \mathcal{F}}{\partial e_i^\alpha \partial e_j^\beta \partial u_k^\mu} = -\frac{1}{2\pi} \text{Im} \text{Tr} \int^{E_F} dE \times \left[\underline{\underline{\tau}}_i^\alpha \underline{\underline{\tau}}_{ij} \underline{\underline{\tau}}_j^\beta \underline{\underline{\tau}}_{jk} \mathcal{U}_k^\mu \underline{\underline{\tau}}_{ki} + \underline{\underline{\tau}}_i^\alpha \underline{\underline{\tau}}_{ik} \mathcal{U}_k^\mu \underline{\underline{\tau}}_{kj} \underline{\underline{\tau}}_j^\beta \underline{\underline{\tau}}_{ji} \right] \quad (15)$$

The displacement operator in Eq. (14) is given by the expression[31]

$$\underline{\underline{\mathcal{U}}}_k^\mu = \bar{U}(\hat{u}_k^\mu) \underline{\underline{m}}_k + \underline{\underline{m}}_k \bar{U}(-\hat{u}_k^\mu), \quad (16)$$

where

$$\bar{U}_{LL'}(\hat{u}_k) = \kappa \frac{4\pi}{3} i^{l+1-l'} \sum_{m=-1}^1 C_{LL'1m} Y_{1m}(\hat{u}_k)$$

and $\kappa = \sqrt{2mE/\hbar^2}$. The prefactor 1/2 occurs to avoid double counting of the identical terms upon summations in Eq.(1) over indices i and j . In a similar way, higher order terms can be expressed. The Fourier transforms of these parameters give access to the investigations of the impact of spin-lattice interactions on magnon and phonon modes (see Appendix B). Note however, that the SLC parameters given by Eq. (15) do not account for the impact of screening of the atomic displacement due to the charge redistribution. To make sure that this contribution can be neglected with a reasonable accuracy of the results, additional calculations discussed in Section IIB have been performed to calculate the J_{ij} parameters for the distorted lattice.

Note that here we focus on the three-site exchange-like contributions to Eq. (1), while a detailed discussion and benchmarking of the three-site approximation is presented in a complementary work [50]. This includes in particular technical details of higher order extensions to Eq. (1). Moreover, an expression for the SLC parameters that describe a modification of the mageto-cryslaline anisotropy due to atomic displacements is presented and discussed together with corresponding numerical results.

III. RESULTS FOR THE EMBEDDED CLUSTER APPROACH

In this section the properties of the SLC parameters obtained via the perturbative SLC method of Mankovsky et al. [31] and via the new method based on embedded cluster (EC) calculations are presented for bcc Fe. As for the supercell method the SLC $J_{ij}^{\alpha\beta,\mu}$ are obtained by the modification of the SSC $J_{ij}^{\alpha\beta}$ in the presence of a vanishingly small displacement u_k^μ [30] (see Fig. 1 and Eq. (2)) after a self-consistent (SCF) calculation of the potential for this distorted geometry has been done.

As mentioned above the cluster method has the advantage that it is accurate for finite cluster sizes, as long as the cluster is large enough to take into account the relaxation effects. This is already the case for relatively small

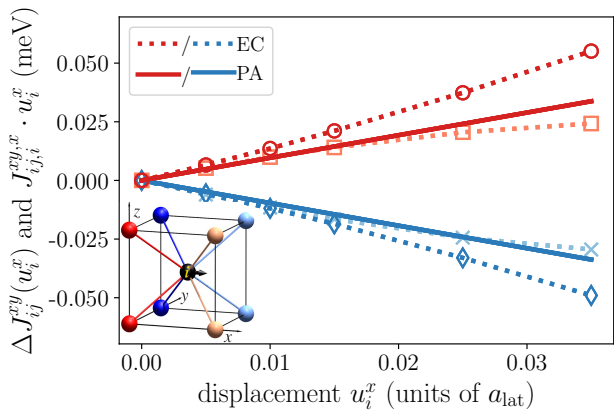


Figure 2. Comparison of the off-diagonal exchange coupling modification of nearest neighbors for embedded clusters (EC) with 27 atoms $\Delta J_{ij}^{xy}(u_i^x) = J_{ij}^{xy}(u_i^x) - J_{ij}^{xy}(0)$ (dotted lines) and the perturbative approach (PA) $J_{ij,i}^{xy,x} \cdot u_i^x$ (solid lines), for a displacement of atom i in x direction for nearest neighbors ij in bcc Fe. The color code for the atoms j is visualized in the inset figure: Dark red circles denote neighbors with $\mathbf{r}_{ij} = a(-0.5, -0.5, \pm 0.5)$, light red squares $\mathbf{r}_{ij} = a(0.5, -0.5, \pm 0.5)$, dark blue diamonds $\mathbf{r}_{ij} = a(-0.5, 0.5, \pm 0.5)$ and light blue crosses $\mathbf{r}_{ij} = a(0.5, 0.5, \pm 0.5)$.

system sizes, as can be seen in Tab. I, which shows that the results for diagonal and off-diagonal SLC parameters obtained from clusters consisting of 16 and 51 atoms are in very good agreement. In contrast, the top of table I shows that this is not the case for supercells consisting of 16 and 54 atoms. The supercell approach is in principle only accurate for infinite supercells since for finite sizes not only a single displaced atom is considered, but a periodic displacement for one atom in each supercell.

Figures 2 and 3 as well as table I compare the results for nearest neighbors and $i = k$ obtained from supercell, cluster and perturbative SLC methods. More results for next-nearest neighbors and other SLC components are presented in Appendix A. In Fig. 3 the modification of the cluster SSC occurring in Eq. (2), i.e. $\Delta J_{ij}^{\alpha\beta}(u_k^\mu) = J_{ij}^{\alpha\beta}(u_k^\mu) - J_{ij}^{\alpha\beta}(0)$ is compared to the perturbative SLC result $J_{ij,k}^{\alpha\beta,\mu} \cdot u_k^\mu$ for $\alpha = \beta = \mu = x$. For small displacements, both results are in good agreement. The average value of the diagonal components $J_{ij,i}^{\text{diag-s},x} = \frac{1}{2}(J_{ij,i}^{x,x,x} + J_{ij,i}^{y,y,x})$ is presented in Tab. I. Again, we find a good agreement between cluster and perturbative SLC results: The average absolute value for the large (small) cluster and nearest neighbors is 8.30 ± 0.22 meV/a.u. (8.28 ± 0.22 meV/a.u.), compared to 9.80 meV/a.u. from the perturbative SLC method. The supercell results for the diagonal SLC are smaller with 7.02 ± 0.42 meV/a.u. (6.91 ± 0.23 meV/a.u.) for large (small) supercells. Similarly, the off-diagonal elements are in good agreement for all methods.

The different values for different neighbors j for both diagonal and off-diagonal components result primarily

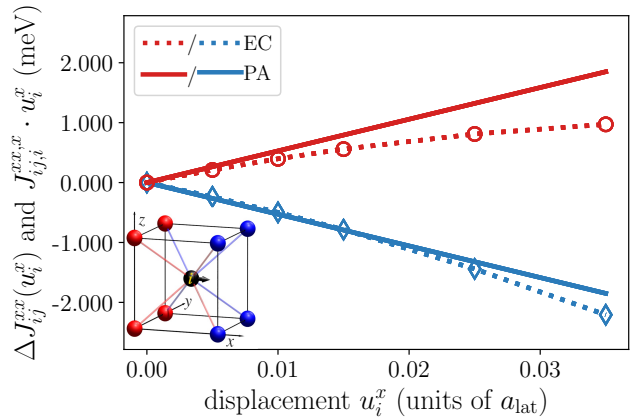


Figure 3. Comparison of the diagonal exchange coupling modification of nearest neighbors for embedded clusters (EC) with 27 atoms $\Delta J_{ij}^{xx}(u_i^x) = J_{ij}^{xx}(u_i^x) - J_{ij}^{xx}(0)$ (dotted lines) and the perturbative approach (PA) $J_{ij,i}^{xx,x} \cdot u_i^x$ (solid lines), for a displacement of atom i in x direction for nearest neighbors ij in bcc Fe. The color code of the atoms j is visualized in the inset figure: Red circles correspond to neighbors with $\mathbf{r}_{ij} = a(-0.5, \pm(\mp)0.5, \pm 0.5)$ and blue diamonds to $\mathbf{r}_{ij} = a(0.5, \pm(\mp)0.5, \pm 0.5)$.

from higher order contributions taken into account by modifications of the electronic structure due to the displacements in clusters and supercells, but not in the perturbative approach. The results for the second neighbor shell are given in the Appendix A. One can see a larger discrepancy between the cluster and PA results, that can be associated with the important role of the screening effects in the exchange interactions at bigger distances indicating a long-range charge density redistribution around displaced atom.

To conclude, the embedded cluster method enables a very accurate calculation of the SLC parameters that can be used to benchmark the perturbative approach. We have shown that the results for bcc Fe agree well for both approaches.

IV. ANALYSIS OF RELATIVISTIC SPIN-LATTICE EXCHANGE COUPLING TENSORS

In this section, we will evaluate the connection of the spin-lattice exchange coupling tensors w.r.t. the crystal symmetry and dipole-dipole contributions based on analytical arguments, before discussing the numerical results in the next section.

$J_{ij,i}^{\text{diag},x}$	supercells		clusters		PA
	16 atoms	54 atoms	27 atoms	51 atoms	
$(-\frac{1}{2}, -\frac{1}{2}, \pm\frac{1}{2})$	6.432	6.37	7.80	7.83	9.80
$(-\frac{1}{2}, \frac{1}{2}, \pm\frac{1}{2})$	6.432	6.37	7.82	7.84	9.80
$(\frac{1}{2}, -\frac{1}{2}, \pm\frac{1}{2})$	-7.397	-7.67	-8.76	-8.77	-9.80
$(\frac{1}{2}, \frac{1}{2}, \pm\frac{1}{2})$	-7.397	-7.67	-8.74	-8.76	-9.80

$J_{ij,i}^{\text{off},x}$	supercells		clusters		PA
	16 atoms	54 atoms	27 atoms	51 atoms	
$(-\frac{1}{2}, -\frac{1}{2}, \pm\frac{1}{2})$	0.23	0.21	0.26	0.25	0.20
$(-\frac{1}{2}, \frac{1}{2}, \pm\frac{1}{2})$	-0.23	-0.21	-0.22	-0.22	-0.20
$(\frac{1}{2}, -\frac{1}{2}, \pm\frac{1}{2})$	0.21	0.19	0.21	0.21	0.20
$(\frac{1}{2}, \frac{1}{2}, \pm\frac{1}{2})$	-0.21	-0.19	-0.24	-0.24	-0.20

Table I. Average absolute value of the diagonal SLC parameters $J_{ij,i}^{\text{diag},x} = \frac{1}{2}(J_{ij,i}^{xx,x} + J_{ij,i}^{yy,x})$ (top) and $J_{ij,i}^{\text{off},x} = \frac{1}{2}(J_{ij,i}^{xy,x} + J_{ij,i}^{yx,x})$ (bottom) in meV/a.u. for nearest neighbors, $i = k$ and a displacement in x direction in bcc Fe obtained by the supercell method for supercells with 16 and 54 atoms, by the embedded cluster (EC) method for clusters with 27 and 51 atoms and for the closed SLC expressions. For the EC calculations $u_i^x = 0.005 a_{\text{lat}}$ was used.

A. Symmetry of the SLC Parameters

The qualitative features of the SLC parameters are determined by the symmetry of the system under investigation. Accordingly, we start our analysis of the spin-lattice exchange coupling tensors by linking their symmetry to the space group of the considered material.

The SLC tensor elements are connected by the relation

$$J_{ij,k}^{\alpha\beta,\mu} = \sum_{\alpha'\beta',\mu'} J_{i'j',k'}^{\alpha'\beta',\mu'} D(R)_{\alpha'\alpha} D(R)_{\beta'\beta} D(R)_{\mu'\mu} \quad (17)$$

for unitary and antiunitary symmetry transformations of the crystal, $u = \{R, \mathbf{p}\}$ and $a = T\{R, \mathbf{p}\}$ respectively, with R denoting a rotation operation, \mathbf{p} a primitive translation operation, T the time inversion operation and $\underline{D}(R)$ the 3×3 matrix representation of R . The original and transformed site positions \mathbf{r}_i and $\mathbf{r}_{i'}$ are related by $\mathbf{r}_{i'} = R\mathbf{r}_i + \mathbf{p}$. Eq. (17) can explain many of the SLC properties observed in the previous section. As an example, we focus on next-nearest neighbors in bcc Fe, with the SLC presented in Appendix A since they lie in x , y , z directions in space and not in the diagonal directions like the nearest neighbors. For example, for R being a 4-fold rotation around the z axis the matrix representation is given by

$$\underline{D}(R) = \begin{pmatrix} 0 & -1 & 0 \\ 1 & 0 & 0 \\ 0 & 0 & 1 \end{pmatrix}.$$

Eq. (17) yields for $r_{ij} = (1, 0, 0)^T$ and $i = k$

$$J_{ij,k}^{xy,x} = J_{i'j',k'}^{yx,y} \cdot 1 \cdot (-1) \cdot 1 = -J_{i'j',k'}^{yx,y}$$

with $r_{i'j'} = (0, 1, 0)^T$. A similar argument holds for $J_{ij,k}^{yx,x}$ and $J_{ij,k}^{xy,y}$, as well as for the off-diagonal components $J_{ij,i}^{\text{off},x}$ and $J_{ij,i}^{\text{off},y}$. This is in agreement with table VII. Furthermore, the relation can explain vanishing components in tables VII in Appendix A, e.g. for $r_{ij} = (1, 0, 0)^T$ and $i = k$, for which a 2-fold rotation around the z axis yields $J_{ij,k}^{xx,z} = J_{i'j',k'}^{xx,z}$, but an inversion implies $J_{ij,k}^{xx,z} = -J_{i'j',k'}^{xx,z}$ for $r_{i'j'} = (-1, 0, 0)^T$. Consequently, $J_{ij,k}^{xx,z} = J_{i'j',k'}^{xx,z} = 0$.

In the following, we proof the symmetry relation (17), starting with the expression for the SLC tensor as given in (15):

$$J_{ij,k}^{\alpha\beta,\mu} = \frac{1}{2\pi} \text{Im} \int^{E_{\text{F}}} dE [j_{ij,k}^{\alpha\beta\mu,1} + j_{ij,k}^{\alpha\beta\mu,2}] \quad (18)$$

with

$$j_{ij,k}^{\alpha\beta\mu,1} = \text{Tr} \mathcal{T}_i^\alpha \tau_{ij} \mathcal{T}_j^\beta \tau_{jk} \mathcal{U}_k^\mu \tau_{ki} \quad (19)$$

and

$$j_{ij,k}^{\alpha\beta\mu,2} = \text{Tr} \mathcal{T}_i^\alpha \tau_{ik} \mathcal{U}_k^\mu \tau_{kj} \mathcal{T}_j^\beta \tau_{ji}. \quad (20)$$

For an arbitrary (unitary or antiunitary) symmetry operation s the first part becomes

$$j_{ij,k}^{\alpha\beta\mu,1} = \text{Tr} \tilde{\mathcal{T}}_i^\alpha \tilde{\tau}_{ij} \tilde{\mathcal{T}}_j^\beta \tilde{\tau}_{jk} \tilde{\mathcal{U}}_k^\mu \tilde{\tau}_{ki}$$

with $\tilde{\mathcal{O}}_i^\alpha = s \mathcal{O}_i^\alpha s^{-1}$. The scattering path operators τ , torque operators \mathcal{T} and displacement operators \mathcal{U} behave under the different types of symmetry operations as follows:

For an unitary symmetry operation u that transforms site $i(j)$ to $i'(j')$ the scattering path operator τ transformations as $u\tau_{ij}u^{-1} = \tau_{i'j'}$ while for an antiunitary symmetry one has [51] $a\tau_{ij}a^{-1} = \tau_{j'i'}^\dagger$. As pointed out in Ref. [52], an arbitrary pseudovector transforms under a symmetry operation $s = \{R, \mathbf{p}\}$ or $s = T\{R, \mathbf{p}\}$ as

$$s\mathbf{v}(\mathbf{r}) = \pm \det(\underline{D}(R)) \underline{D}(R)\mathbf{v}(s^{-1}\mathbf{r})$$

while a vector transforms like

$$s\mathbf{v}(\mathbf{r}) = \pm \underline{D}(R)\mathbf{v}(s^{-1}\mathbf{r}).$$

In these expressions the sign \pm is determined by the behavior of \mathbf{v} under time reversal: the positive sign applies for (polar) vectors and the negative sign for (axial) pseudovectors [52]. As the torque operator $\tilde{\mathcal{T}}$ behaves as a pseudovector the sign \pm and $\det(\underline{D}(R)) = \pm 1$ from the first expression occur twice in Eq. (20), and hence cancel each other. Consequently, one finds

$$\tilde{\mathcal{T}}_i^\alpha \dots \tilde{\mathcal{T}}_j^\beta = \sum_{\alpha'\beta'} \mathcal{T}_{i'}^{\alpha'} \dots \mathcal{T}_{j'}^{\beta'} D(R)_{\alpha'\alpha} D(R)_{\beta'\beta}. \quad (21)$$

For the displacement operator, which is not affected by time reversal, we have a positive sign and hence

$$\tilde{\mathcal{U}}_k^\mu = \sum_{\mu'} \mathcal{U}_{k'}^{\mu'} D(R)_{\mu'\mu}. \quad (22)$$

		Fe ($r_{ij} = 0.87$)	Fe ($r_{ij} = 1$)	MnGe	Au on Fe	
SSC	$J_{ij}^{\text{diag-s}}$	18.051	10.090	18.187	21.414	
	$J_{ij}^{\text{diag-a}}$	0.0	0.015	0.009	0.0091	
	$J_{ij}^{\text{off-s,x}}$	0.013	0.0	0.012	0.079	
	$ D_{ij}^x $	0.0	0.0	0.151	0.272	
	$J_{ij,\text{dip}}^{\text{diag-s}}$	0.0	0.013	0.004	0.006	
	$J_{ij,\text{dip}}^{\text{diag-a}}$	0.00	0.039	0.006	0.008	
	$J_{ij,\text{dip}}^{\text{off-s,x}}$	0.040	0.0	0.008	0.015	
	$ D_{ij,\text{dip}}^x $	0.0	0.0	0.0	0.0	
	SLC	$J_{ij,i}^{\text{diag-s}}$	9.792	1.858	9.792	7.693
		$J_{ij,i}^{\text{diag-a}}$	0.012	0.010	0.010	0.020
$J_{ij,i}^{\text{off-s,x}}$		0.019	0.007	0.009	0.013	
$ D_{ij,i}^x $		0.197	0.380	0.618	2.941	
$J_{ij,i,\text{dip}}^{\text{diag-s}}$		0.023	0.034	0.007	0.011	
$J_{ij,i,\text{dip}}^{\text{diag-a}}$		0.070	0.102	0.015	0.033	
$J_{ij,i,\text{dip}}^{\text{off-s,x}}$		0.046	0.068	0.013	0.005	
$ D_{ij,i,\text{dip}}^x $		0.0	0.0	0.0	0.0	

Table II. Maximal dipole-dipole contributions for SSC (top) and SLC (bottom) exchange couplings of different materials: bulk Fe, MnGe for Mn atoms at sites i and j ($r_{ij} = 0.61$) and three layers of gold on iron (Au on Fe) for Fe atoms at sites i and j ($r_{ij} = 0.71$). For the dipole-dipole interactions we use for the anti-symmetric off-diagonal elements the same notation as for DMI-like parameters, i.e. $D_{ij(i),\text{dip}}$. From Eq. (23) it directly follows that the anti-symmetric off-diagonal elements of both tensors (and hence the DMI and SLC-DMI) vanish for all materials.

For unitary operations this yields

$$j_{ijk}^{\alpha\beta\mu,1} = \sum_{\alpha'\beta'\mu'} j_{i'j'k'}^{\alpha'\beta'\mu',1} D(R)_{\alpha'\alpha} D(R)_{\beta'\beta} D(R)_{\mu'\mu}.$$

For antiunitary operations we find

$$j_{ijk}^{\alpha\beta\mu,1} = \sum_{\alpha'\beta'\mu'} j_{i'j'k'}^{\alpha'\beta'\mu',2} D(R)_{\alpha'\alpha} D(R)_{\beta'\beta} D(R)_{\mu'\mu}$$

and

$$j_{ijk}^{\alpha\beta\mu,2} = \sum_{\alpha'\beta'\mu'} j_{i'j'k'}^{\alpha'\beta'\mu',1} D(R)_{\alpha'\alpha} D(R)_{\beta'\beta} D(R)_{\mu'\mu}.$$

Hence, the same relation for unitary as well as antiunitary symmetry operations holds.

B. Dipole-Dipole Contribution to SLC

In order to have a complete picture of the spin-lattice interactions in magnetic materials the contribution to the SSC and SLC tensors from the dipole-dipole interaction is considered. Although the dipole-dipole interaction is treated on a classical level, represented by the Hamiltonian

$$H_{\text{dip}} = -\frac{\mu_0}{4\pi|\mathbf{r}_{ij}|^3} [3(\mathbf{m}_i \cdot \hat{\mathbf{r}}_{ij})(\mathbf{m}_j \cdot \hat{\mathbf{r}}_{ij}) - \mathbf{m}_i \cdot \mathbf{m}_j], \quad (23)$$

for two magnetic moments \mathbf{m}_i and \mathbf{m}_j at sites i and j separated by a distance vector \mathbf{r}_{ij} , its contribution arises from the (quantum-electro-dynamical) Breit interaction [53]. Consequently, it can be considered as a consistent addition to the exchange coupling tensors presented in the previous sections. For a ferromagnetic reference system with $\mathbf{m}_i \parallel \mathbf{e}_z$ the SSC contribution is given by

$$J_{ij,\text{dip}}^{xx} = -\frac{\mu_0}{4\pi|\mathbf{r}_{ij}|^3} m_i^{z,0} m_j^{z,0} [3(\hat{r}_{ij}^x)^2 - 1]$$

$$J_{ij,\text{dip}}^{yy} = -\frac{\mu_0}{4\pi|\mathbf{r}_{ij}|^3} m_i^{z,0} m_j^{z,0} [3(\hat{r}_{ij}^y)^2 - 1]$$

$$J_{ij,\text{dip}}^{xy} = J_{ij,\text{dip}}^{yx} = -\frac{\mu_0}{4\pi|\mathbf{r}_{ij}|^3} m_i^{z,0} m_j^{z,0} 3\hat{r}_{ij}^x \hat{r}_{ij}^y$$

and the SLC contribution, here for a displacement in $\mu = x$ direction, is

$$J_{ij,\text{dip}}^{xxx} = -\frac{3\mu_0}{4\pi} m_i^{z,0} m_j^{z,0} \frac{3r_{ij}^x((r_{ij}^y)^2 + (r_{ij}^z)^2) - 2(r_{ij}^x)^3}{|\mathbf{r}_{ij}|^7}$$

$$J_{ij,\text{dip}}^{yyy} = -\frac{3\mu_0}{4\pi} m_i^{z,0} m_j^{z,0} \frac{r_{ij}^x((r_{ij}^x)^2 - 4(r_{ij}^y)^2 + (r_{ij}^z)^2)}{|\mathbf{r}_{ij}|^7}$$

$$\begin{aligned} J_{ij,\text{dip}}^{xyx} &= J_{ij,\text{dip}}^{yxx} \\ &= \frac{3\mu_0}{4\pi} m_i^{z,0} m_j^{z,0} \frac{r_{ij}^y(4(r_{ij}^x)^2 - (r_{ij}^y)^2 - (r_{ij}^z)^2)}{|\mathbf{r}_{ij}|^7}. \end{aligned}$$

The dipole-dipole contribution is normally considered to be very small and negligible. Exemplary values are shown in Tab. II. It can be seen that the dipole-dipole contribution is even larger than the values obtained from the perturbative method for some SSC as well as SLC components for some of the materials considered.

To conclude, we have shown that dipole-dipole interactions can make – depending on the material under consideration – a significant contribution to the SLC parameters. This is particularly interesting for the simulation of these materials, e.g. via combined spin-lattice molecular dynamics (MD) simulations: When modeling the combined spin and lattice dynamics, the largest SLC contributions should be taken into account preferentially. Our results show that one has to carefully consider the various contributions for each material. In particular, we have shown that for some materials the dipole-dipole interaction may even play a leading role, as it has already been assumed in spin-lattice MD simulations, e.g. by Aßmann et al. [25] or Strungaru et al. [28].

V. NUMERICAL RESULTS

A. SLC Tensors for collinear ferro- and antiferromagnets

Here, we will analyze the SLC parameters systematically for various materials with different magnetic structures, investigate the role of spin-orbit coupling, and

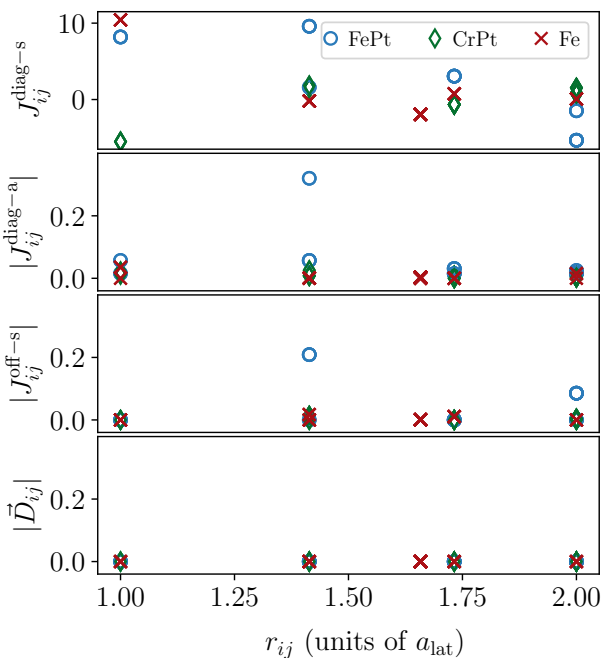


Figure 4. SSC contributions in FePt (circles) and CrPt (diamonds) for atoms i and j being Fe / Cr atoms, compared to the values for bcc Fe (crosses). FePt is ferromagnetic and hence the isotropic part $J_{ij}^{\text{diag-s}} = \frac{1}{2}(J_{ij}^{xx} + J_{ij}^{zz})$ is positive. FePt is anisotropic in z direction, i.e. the diagonal anti-symmetric part $J_{ij}^{\text{diag-a}} = \frac{1}{2}(J_{ij}^{xx} - J_{ij}^{zz})$ is relatively large. The off-diagonal symmetric part is given by $J_{ij}^{\text{off-s}} = \frac{1}{2}(J_{ij}^{xy} + J_{ij}^{yx})$.

compare the SLC contributions for bulk geometries and free standing monolayers as well as different substrate materials for deposited magnetic films. Furthermore, we will shine light on the role of different elements on the strength of spin-lattice interactions. Finally, we show that the resulting SLC contributions can be connected to modifications of the phonon dispersion due to spin-lattice coupling as proposed by Ref. [31]. If not stated differently calculations are performed using LDA-DFT with a k -mesh of 2000 points and $l_{\text{max}} = 3$.

1. Dependence on Magnetic Structure: FePt vs. CrPt

FePt and CrPt have a very similar lattice structure, both being ordered in the $L1_0$ phase. The lattice constants are $a_{\text{lat}}^{\text{FePt}} = 2.72 \text{ \AA}$ and $a_{\text{lat}}^{\text{CrPt}} = 2.67 \text{ \AA}$. However, the magnetic properties of both materials are very different. This can be observed in Fig. 4: Whereas FePt is ferromagnetic with strong FM nearest neighbor Fe-Fe interactions, with $J_{ij}^{\text{diag-s}} = 8.5 \text{ meV}$ for in-plane neighbors, CrPt is strongly antiferromagnetic with negative nearest Cr neighbor coupling $J_{ij}^{\text{diag-s}} = -4.4 \text{ meV}$ for in-plane neighbors [55]. The induced magnetic moment of Pt is rather small and hence also the respective SSC with Pt at

sites i or j are small [56]. Both materials are anisotropic in z direction with a diagonal anti-symmetric part up to $|J_{ij}^{\text{diag-a}}| = \frac{1}{2}|J_{ij}^{xx} - J_{ij}^{zz}| = 0.32 \text{ meV}$ in FePt and $|J_{ij}^{\text{diag-a}}| = 0.026 \text{ meV}$ in CrPt for out-of-plane neighbors, which is relatively large compared to the DMI and symmetric off-diagonal contributions.

In Fig. 5 the SLC parameters for FePt and CrPt are presented. In the case of FePt the isotropic SLC part decays exponentially, starting from $|J_{ij,j}^{\text{diag-s,x}}| = \frac{1}{3}|J_{ij,j}^{xx} + J_{ij,j}^{zz}| = 12.8 \text{ meV/a.u.}$ for neighboring Fe atoms. The same behavior is observed for CrPt with slightly smaller isotropic parts up to $|J_{ij,j}^{\text{diag-s,x}}| = 8.6 \text{ meV/a.u.}$ for neighboring Cr atoms. Note that $J_{ij,j}^{\text{diag-s,x}}$ can be positive and negative for ferromagnetic as well as antiferromagnetic materials, depending on the position of atom j w.r.t. the displaced atom i . The second-largest SLC contributions are the on-site anti-symmetric diagonal parts and the DMI contribution (both around 4% of the isotropic part) for nearest Fe sites in FePt and the DMI contribution (around 0.6% of the isotropic part) in CrPt for nearest Cr neighbors. However, there is a relatively large SLC-DMI contribution for neighbors with $r_{ij} = (0, 1.0, 1.4) a_{\text{lat}}$, e.g. with $|D_{ij,j}^x| = \frac{1}{2}|J_{ij,j}^{yz} - J_{ij,j}^{zy}| = 0.58 \text{ meV/a.u.}$ ($|D_{ij,j}^x| = 0.28 \text{ meV/a.u.}$) compared to $|J_{ij,j}^{\text{diag-s,x}}| = 0 \text{ meV/a.u.}$

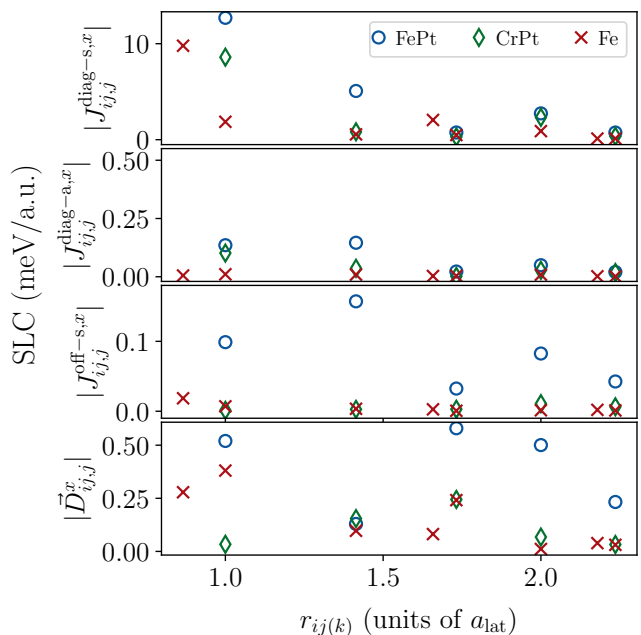


Figure 5. Maximal SLC contributions for each distance r_{ij} in FePt (empty circles) and CrPt (filled diamonds) for atoms i and j being Fe / Cr atoms, compared to the values for bcc Fe presented in Ref. [54] (crosses). FePt as well as CrPt has a large anisotropy in z direction, i.e. the anti-symmetric part of the diagonal components $J_{ij,k}^{\text{diag-a},\mu} = \frac{1}{2}(J_{ij,k}^{xx,\mu} - J_{ij,k}^{zz,\mu})$ is relatively large.

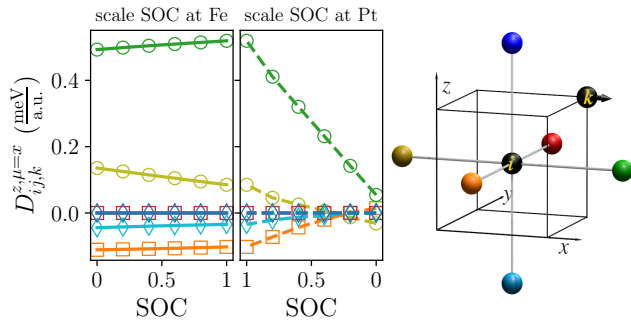


Figure 6. Dependence of SLC-DMI $D_{ij,k}^{z,\mu=x}$ in FePt for all nearest neighbors on the strength of SOC, scaled at the Fe (left) or Pt (right) sites, for iron atoms at sites i and j . The displaced atom is a Pt atom with $r_{ik} = (0.5, 0.5, 0.5) a_{\text{lat}}$.

for the same neighbors or $|J_{ij,j}^{\text{diag-s},x}| = 0.65 \text{ meV/a.u.}$ ($|J_{ij,j}^{\text{diag-s},x}| = 0.29 \text{ meV/a.u.}$) for other neighbors with the same distance from atom i for FePt (CrPt). Compared to Fe, the SLC-DMI values are in the same order of magnitude, whereas the anisotropic parts of bcc Fe $J_{ij}^{\text{diag-a}}$ and $J_{ij,j}^{\text{diag-a}}$ are much smaller. Note that here we consider the asymmetry of the diagonal parameters between x and z directions, instead of x and y considered in Ref. [31]. Hence, it seems that a material with strong magnetic anisotropy (i.e. large $J_{ij}^{\text{diag-a}}$) has an anti-symmetric diagonal part which is more affected by the displacement than for materials with small anisotropy parts.

Since the SPRKKR program [57] used for the present investigations allows to scale the strength of the relativistic spin-orbit correction, it is possible to investigate the role of the SOC on the atoms which mediate the SLC interaction. This is shown in Fig. 6. It presents the effect of the SOC on the SLC for nearest Fe neighbors (left) and on pairs of Fe atoms i and j up to $r_{ij} \leq 2 a_{\text{lat}}$ for a lattice distortion at a Pt site k with $r_{ik} = (0.50, 0.50, 1.41) a_{\text{lat}}$ (right). It can be seen that the SLC-DMI exhibits only a weak dependence on the strength of the SOC at the Fe sites, but a strong dependence on the SOC of the Pt atoms: The z -component of the SLC-DMI decreases by almost one order of magnitude when the SOC on the mediating Pt atom is scaled to zero. This indicates that the mediating atoms play a key role for the influence of the spin-lattice coupling.

2. Dependence on Dimensionality: Bulk Iron, Free Standing Iron Monolayer and Substrates

Here, we compare the SSC and SLC parameters for materials with different dimensionality. We will compare the exchange interactions for bulk Fe, free standing monolayers with their surface perpendicular to the [001] and [111] directions and substrate materials with a Fe

SSC	bulk Fe	Fe(001)	Fe(111)	Fe on Ir
$J_{ij}^{\text{diag-s}}$	11.39	25.29	24.02	7.35
$J_{ij}^{\text{diag-a}}$	0.00	0.05	0.03	0.07
$J_{ij}^{\text{off-s}}$	0.01	0.00	0.03	0.08
D_{ij}^z	0.00	0.00	0.00	1.84

Table III. Maximal absolute SSC contributions in meV in bulk Fe, free standing monolayers with their surface perpendicular to the [001] and [111] directions and a deposited Fe film on Ir with its surface perpendicular to the [111] direction. Note that the contributions come from different neighbors with different distances, not necessarily nearest neighbors.

SLC	μ	bulk Fe	Fe(001)	Fe(111)	Fe on Ir
$J_{ij,j}^{\text{diag-s},\mu}$	x	9.79	18.90	32.09	10.80
	y	9.79	18.90	27.79	10.54
	z	9.79	0.09	0.29	9.61
$J_{ij,j}^{\text{diag-a},\mu}$	x	0.01	0.22	0.03	0.15
	y	0.01	0.27	0.03	0.17
	z	0.01	0.03	0.0	0.15
$J_{ij,j}^{\text{off-s},\mu}$	x	0.02	0.05	0.03	0.14
	y	0.02	0.05	0.04	0.12
	z	0.02	0.00	0.0	0.15
$D_{ij,j}^{z,\mu}$	x	0.38	0.47	0.28	2.62
	y	0.38	0.47	0.33	2.28
	z	0.04	0.00	0.30	0.31

Table IV. Maximal absolute SLC contributions for $j = k$ and displacement in x direction in meV/a.u. in bulk Fe, free standing monolayers with their surface perpendicular to the [001] and [111] directions and a deposited Fe film on Ir with its surface perpendicular to the [111] direction.

layer deposited on a metal $M(111)$ surface and $M = \text{Ir}$. From tables III and IV it can be seen that the dimensionality of the considered material affects both SSC and SLC significantly: For the SSC, the isotropic exchange of the two dimensional free-standing film is more than twice as large as for the bulk material. Apart from that, all other contributions vanish or are much smaller than the isotropic part in both materials. In contrast, the SLC have other significant contributions to the SLC tensor apart from the isotropic exchange. In both materials the SLC-DMI $D_{ij,j}^{\mu}$ is the second largest contribution to the SLC tensor, as reported for bulk Fe by Ref. [31]. Even when comparing to the SSC contributions, $D_{ij,j}^{\mu} \cdot u_j^{\mu}$ gives the second largest energy contribution for a realistic displacement of e.g. around 2% of the lattice constant. This term hence can significantly contribute to angular momentum transfer between the spin system and the lattice. An exception is the SLC-DMI contribution for an out-of plane displacement $D_{ij,j}^z$ for Fe(001). Furthermore, there is a relatively large SLC anisotropic part $J_{ij,j}^{\text{diag-a},x}$ and $J_{ij,j}^{\text{diag-a},y}$ in the monolayer, but not in the bulk material, which can also be related to spin-lattice angular momentum transfer. Note that the contributions in tables III and IV come from different neighbors with different distances, not necessarily nearest neighbors.

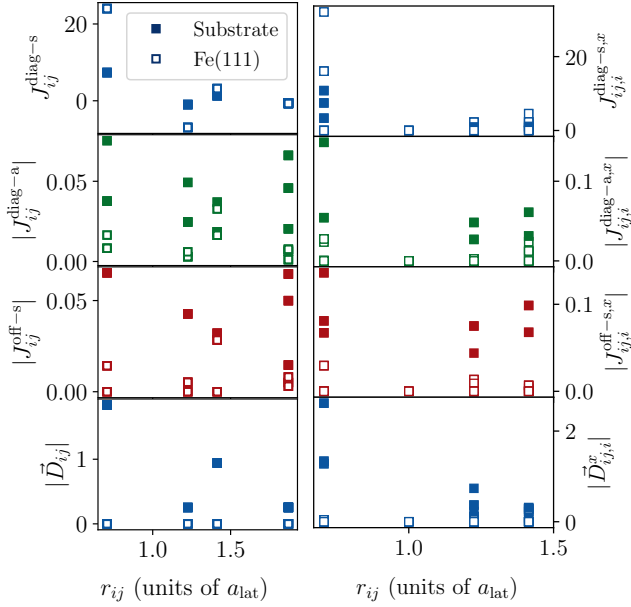


Figure 7. Comparison of SLC contributions for a surface layer system consisting of a Fe monolayer on Ir(111) and a free standing Fe(111) monolayer. Sites i and j are occupied by a Fe atom.

For bulk Fe, displacements in x , y and z directions have the same maximal absolute contributions. Note, however, that this symmetry is actually broken since the magnetization direction (here: z direction) is taken into account. This becomes clear when considering the individual tensor elements, with e.g. $J_{ij,j}^{xy,x} = 0.22 \frac{\text{meV}}{\text{a.u.}} \neq J_{ij,j}^{xy,z} = 0.02 \frac{\text{meV}}{\text{a.u.}}$. In the monolayer, where the magnetization is aligned in the out-of-plane direction, the asymmetry of x/y directions compared to the z direction is much larger and can also be observed in the maximal SLC tensor contributions in Tab. IV.

The effect of the dimensionality of the considered system on the SSC and SLC contributions can also be observed when investigating the transition between 2D monolayers to substrate system consisting of a Fe monolayer with its surface perpendicular to (111) on three layers of a metal (here Ir). The respective spin-spin and spin-lattice exchange coupling contributions for i being a Fe atom and $i = k$ are shown in tables III and IV as well as in Fig. 7. Further details on the calculations can be found in the next section. It can be seen that the results for the free standing monolayer and the substrate materials strongly differ in the spin-spin and spin-lattice case. For the SSC and SLC isotropic parts, the monolayer has stronger exchange contributions for most configurations of i and j for the SSC and SLC. In contrast, other contributions related to anisotropy and angular momentum transfer [31], are dominated by the substrate material for SSC and SLC and all distances between atoms i and j . In particular, there is a finite z component of the SSC-

displ. μ	M	$D_{ij,i}^{x,\mu}$	$D_{ij,i}^{y,\mu}$	$D_{ij,i}^{z,\mu}$	$ \mathbf{D}_{ij,i}^\mu $
x	Ir	0.49	0.36	2.62	2.69
	Pt	1.23	0.05	0.55	1.35
	Au	0.99	0.44	2.76	2.97
y	Ir	0.31	0.68	2.25	2.37
	Pt	0.60	1.15	0.69	1.46
	Au	1.21	0.22	3.07	3.30
z	Ir	1.77	4.03	0.31	4.41
	Pt	0.11	0.98	0.38	1.06
	Au	0.62	3.56	0.04	3.61

Table V. Absolute values of SLC-DMI in three layers of $M = \text{Ir, Pt, Au}$ on Fe for displacements μ and a Fe atom at sites i and j .

DMI which is related to the lack of inversion symmetry in the substrate. For the monolayer, $D_{ij}^z = 0$ as already presented in Tab. III. Also in the SLC-DMI case the contributions of the substrate dominate.

3. Dependence on Element Types: Substrates

So far we focused on the properties of the SLC parameters $J_{ij,k}$ assuming $k = j$, characterizing the modification of the exchange interactions between the atoms on sites i and j , when one of the atoms is displaced. This however does not imply that an impact of displacements of the atoms on sites $i \neq k \neq j$ can be neglected, although the role of these displacements depends on the material, in particular on the origin of the exchange interaction. To discuss this contribution we consider 2D materials consisting of a Fe monolayer (ML) deposited on a $M(111)$ surface and investigate the role of the type of substrate $M = \text{Ir, Pt, Au}$. The elements Ir, Pt and Au belong to the sixth period of the periodic table and to neighboring groups 9, 10 and 11. Their electronic configurations are $[\text{Xe}] 4f^{14}5d^76s^2$ (Ir), $[\text{Xe}] 4f^{14}5d^96s^1$ (Pt) and $[\text{Xe}] 4f^{14}5d^{10}6s^1$ (Au). We model the system by a 3ML slab, i.e. calculations were performed for a supercell consisting of two vacuum layers, one Fe surface layer and three M layers representing the substrate. Hence, the considered system actually consists of an infinite stack of substrate layers, separated by two vacuum layers. The number of separating vacuum layers between the surface layers is sufficiently large and the interlayer interactions sufficiently small to consider the system as an isolated surface layer-substrate system.

The maximal nearest-neighbor SLC-DMI values for other substrate materials with substrates $M = \text{Ir, Pt and Au}$ are shown in Tab. V. It can be seen that the substrates $M = \text{Ir}$ and $M = \text{Au}$ have a SLC-DMI with similar absolute values and the same largest components for all displacements. For Pt, the results are in general much smaller, with different largest SLC-DMI components.

The contribution of SSC and SLC with Ir atoms as one of the interacting atoms (e.g. atom j in Fig. 7) are

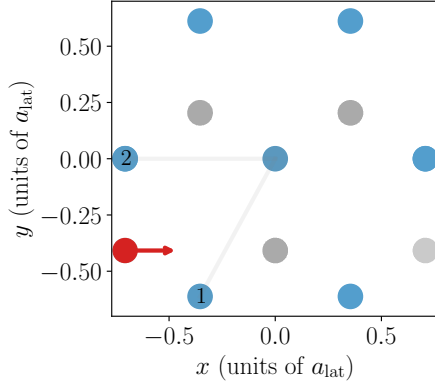


Figure 8. SLC contributions for a surface layer system consisting of a Fe monolayer on Ir(111). Fe atoms are represented by blue dots with the central atom being atom i and atoms 1 (2) being j . The red dot and grey dots represent the displaced and the other Ir atoms in the first substrate layer.

zero due to the vanishing magnetic moment of Ir atoms. However, the configuration of the Ir atoms can strongly affect the spin-lattice exchange strength. This is visualized in Fig. 8 for a specific configuration with an Ir atom (red) located in the first Ir layer on the Fe layer and displaced in x direction. Here, the diagonal SLC contributions are not negligible, i.e. $J_{ij,k}^{\text{diag-s}}(\mathbf{r}_1) = 3.30 \frac{\text{meV}}{\text{a.u.}}$ and $J_{ij,k}^{\text{diag-s}}(\mathbf{r}_2) = -0.40 \frac{\text{meV}}{\text{a.u.}}$. For the z component of the SLC-DMI we find $D_{ij,k}^z(\mathbf{r}_1) = 0.16 \frac{\text{meV}}{\text{a.u.}}$ and $D_{ij,k}^z(\mathbf{r}_2) = 0.39 \frac{\text{meV}}{\text{a.u.}}$.

B. Spin-Lattice Effects in Frustrated Antiferromagnets

As seen in the previous section, the magnetic properties determined by the spin-spin exchange interaction tensor J_{ij} can change significantly when displacing atoms i and j , or a third atom $k \neq i, j$. This becomes particularly interesting in frustrated antiferromagnets where the magnetic configuration depends extremely sensitively on changes of J_{ij} for neighbors j in different directions.

To discuss this issue, we consider in this section the spin-lattice interactions for CuCrO_2 [6] which belongs to a family of triangular lattice antiferromagnets (TLA) ACrO_2 , exhibiting interesting magnetic and magnetoelectric and magnetoelastic properties determined by geometrical spin frustration [4, 58–61]. This compound is characterized by a leading AFM nearest-neighbor (nn) Cr-Cr interaction and weak interactions for an increasing distance between the interacting Cr atoms. As is discussed in the literature, the nn Cr-Cr interactions in these materials may be treated in terms of two competing contributions [4, 62–66]: (a) direct antiferromagnetic interactions of neighboring Cr atoms and (b) indirect fer-

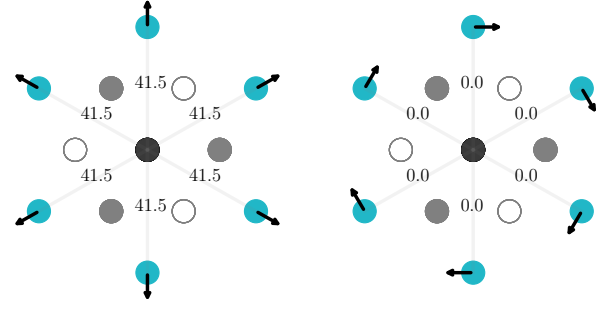


Figure 9. Longitudinal $J_{ij,j}^{\text{diag-s,lng}}$ (left) and transverse $J_{ij,j}^{\text{diag-s,trans}}$ (right) SLC parameters for CuCrO_2 , defined in Eqs. (24) and (25) in $\text{meV}/\text{a.u.}$

romagnetic superexchange interactions mediated by O atoms (since $\text{Cr}_1 - \text{O} - \text{Cr}_2$ form an angle of $\approx 90^\circ$), indicating that the leading contribution is the direct Cr-Cr interaction. As a consequence, different SLC parameters can be contributed by different types of exchange interactions (see Appendix D).

Considering the diagonal symmetric SLC parameters $J_{ij,k}^{\text{diag-s},\mu} = \frac{1}{2}(J_{ij,k}^{xx,\mu} + J_{ij,k}^{yy,\mu})$, the parameters with k characterizing the position of an atom O can be associated mainly with the superexchange mechanism since a displacement of atom O does not change the Cr-Cr distance. On the other hand, the $J_{ij,j}^{\text{diag-s},\mu}$ parameters are connected first of all with the direct exchange.

First we will discuss the properties of the SLC parameters $J_{ij,j}^{\text{diag-s},\mu} = \frac{1}{2}(J_{ij,j}^{xx,\mu} + J_{ij,j}^{yy,\mu})$ corresponding to $k = j$. They characterize the change of the Cr-Cr exchange interaction due to displacement of one of the interacting Cr atoms, or alternatively, they may be seen as the parameters characterizing the force $\mathbf{f}_{ij,j}$ acting on atom j , induced by spin tiltings on sites i and j , having the components $f_{ij,j}^\mu \sim J_{ij,j}^{\text{diag-s},\mu}$. It is instructive to represent the SLC parameters in terms of “longitudinal” and “transverse” displacements, or “longitudinal” and “transverse” induced forces. The “longitudinal” force on atom j relative to atom i is oriented along the $\hat{e}_{ij} = \mathbf{r}_{ij}/|\mathbf{r}_{ij}|$ direction, that gives

$$J_{ij,j}^{\text{diag-s,lng}} = J_{ij,j}^{\text{diag-s,x}}(\hat{x} \cdot \hat{e}_{ij}) + J_{ij,j}^{\text{diag-s,y}}(\hat{y} \cdot \hat{e}_{ij}). \quad (24)$$

The “transverse” forces perpendicular to this direction are characterized by corresponding SLC parameters given by

$$\begin{aligned} J_{ij,j}^{\text{diag-s,trans}} &= J_{ij,j}^{\text{diag-s,x}}(\hat{x} \cdot [\hat{e}_{ij} \times \hat{z}]) \\ &\quad + J_{ij,j}^{\text{diag-s,y}}(\hat{y} \cdot [\hat{e}_{ij} \times \hat{z}]) \\ &= J_{ij,j}^{\text{diag-s,x}}(\hat{y} \cdot \hat{e}_{ij}) - J_{ij,j}^{\text{diag-s,y}}(\hat{x} \cdot \hat{e}_{ij}). \end{aligned} \quad (25)$$

These nearest-neighbor “longitudinal” (left) and “transverse” (right) SLC parameters for CuCrO_2 are shown in Fig. 9. As one can see, the “longitudinal” SLC are finite

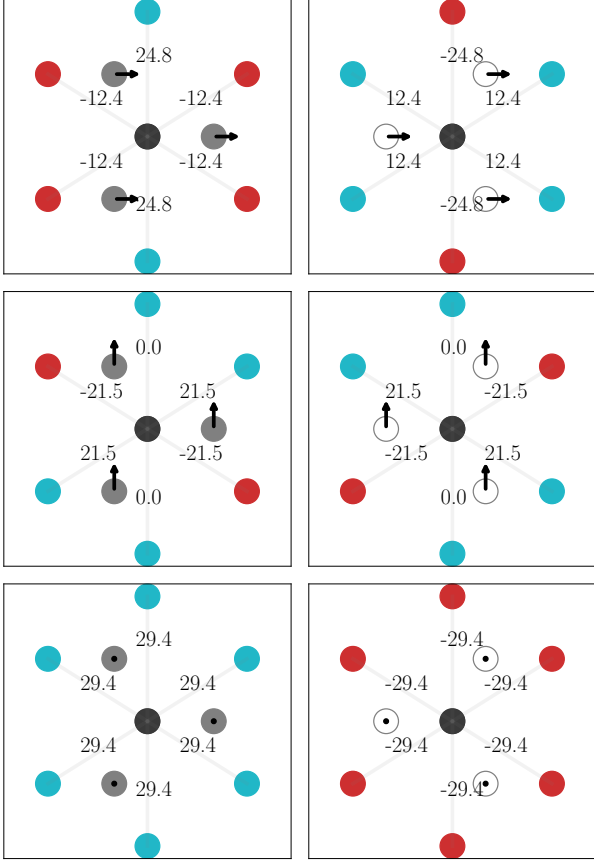


Figure 10. Symmetric SLC $J_{ij,k}^{\text{diag-s},\mu}$ in CuCrO_2 for Cr sites at i and j and for a displacement in $\mu = x, y, z$ directions (first, second, third row) at a O site k in the layer below (solid dots, left column) and above (empty dots, right column) the Cr layer (in meV/a.u.).

and the same for all nearest neighbors, while the “transverse” SLC parameters are equal to zero. This is a consequence of the symmetry of the system including a 3-fold rotation axis as well as σ_{xz} and σ_{yz} mirror planes. This implies that the forces on atoms j in CuCrO_2 , induced by spin tiltings on nearest-neighbor Cr sites via $\mathcal{J}_{ij,j}^{\text{diag-s},\mu}$ interactions are oriented along the lines connecting these two atoms.

As a next step, we discuss the three-site SLC parameters $\mathcal{J}_{ij,k}^{\text{diag-s},\mu}$ corresponding to nearest-neighbor Cr atoms in the positions i and j and the O atom on site k , which originate from the superexchange mechanism (Appendix D). These parameters are presented in figure 10 for $\mu = \{x, y, z\}$. Filled gray circles in the left column correspond to the O layer below and empty circles in the right column correspond to the O layer above the Cr layer in CuCrO_2 . These parameters have the same order of magnitude as the SLC related to the displacement of one of the Cr atoms at $k = j$. Again, one can observe the impact of the crystal symmetry on the SLC parameters, which yields different values for atoms k lo-

μ	x	y	z
	Cr	Cr	Cr
$D_{ij,j}^{x,\mu}$	-0.35	0	-0.15
$D_{ij,j}^{y,\mu}$	0.0	-0.04	0.0
$D_{ij,j}^{z,\mu}$	-0.08	0.0	-0.79

μ	x (a)		y (b)		z (c)	
	O _{top} (l)	O _{bot} (r)	O _{top} (l)	O _{bot} (r)	O _{top} (l)	O _{bot} (r)
$D_{ij,k}^{x,\mu}$	-0.26	-0.26	0	0	-0.21	-0.21
$D_{ij,k}^{y,\mu}$	0	0	0.012	0.012	0	0
$D_{ij,k}^{z,\mu}$	-0.06	-0.06	0	0	0.64	0.64

Table VI. The DMI-like SLC parameters for CuCrO_2 $D_{ij,k}^{\alpha,\mu}$: with the site $k = j$, i.e. occupied by Cr (top) and $k \neq j$, i.e. occupied by O (bottom), for three different directions of displacement of the nearest neighbor Cr and O atoms, i.e. x, y, z (see Fig. 10).

cated above and below the Cr layer. This contribution may be important since it represents the impact of the spin-lattice coupling on the phonon spectra, in addition to the local spin-lattice term [33, 34] describing the interplay of spin degree of freedom with the displacements of the non-magnetic atoms.

In summary, we can see comparable values of the SLC parameters $\mathcal{J}_{ij,k}^{\text{diag-s},\mu}$ in the cases of $k = j$ and $k \neq j$, indicating in general the same significance of both of them for a possible lattice distortion or phonon modes modification concomitant to magnetic ordering in the system.

To complete the discussion, we represent also the properties of the DMI-like SLC parameters for CuCrO_2 . The $\mathcal{D}_{ij,k}^{\alpha,\mu}$ components are presented in Tab. VI for three different directions of displacement x, y, z , respectively for the case $k = j$ (i.e. k site occupied by Cr (top)) and $k \neq j$ (i.e. k site occupied by O (bottom)). For convenience, for every pair of nearest neighbor Cr atoms i and j , one can consider displacements of the O atom within the corresponding planes, either along the \mathbf{R}_{ij} vector or perpendicular to it. Therefore, in both cases, top and bottom, it is sufficient to see the properties of the DMI-like parameters between the Cr atoms connected by vector $\mathbf{R}_{ij} = (0, a, 0)$ (i.e. $\hat{r}_{ij} = \hat{y}$). Again, these parameters can be seen as a measure for the forces on atoms j (top) and k (bottom), induced by spin tiltings via different components of DMI-like SLC. As in the case of diagonal symmetric SLC parameters, one can see that $D_{ij,k}^{\alpha,\mu}$ are comparable in the cases of $k = j$ and $k \neq j, i$ (where the k site occupied by the O atom), while the DMI-like parameters are smaller by about two orders of magnitude.

VI. SUMMARY

To conclude, we have provided a systematic analysis of spin-lattice interactions in collinear ferromagnets and antiferromagnets as well as frustrated AFMs. It

was demonstrated that the crystal structure, the magnetic configuration and the dimensionality of the material under consideration determine the strength of the coupling between the spins and the lattice. Furthermore, relativistic effects give rise to non-vanishing components of the spin-lattice coupling tensor that can be connected to a two-site spin-lattice anisotropy and a spin-lattice Dzyaloshinskii–Moriya interaction. Our results are particularly interesting for modeling magnetic materials via combined spin-lattice molecular dynamics simulations since we show that different contributions to the SLC tensor can be relevant depending on the material under consideration. For some materials, even dipole-dipole interactions may have a significant impact on the SLC parameters.

By calculating the respective spin-lattice interactions for CuCrO_2 compounds, it was demonstrated that the modification of the spin-spin counterparts is significantly large during the structural transition in these systems and hence might give insights into the magnetic transition that happens simultaneously. The results are benchmarked against calculations performed with embedded clusters, which is so far the most accurate scheme to calculate spin-lattice interactions from first principles.

Acknowledgements.– The work in Konstanz was supported by the DFG via project 290/5-2.

- [1] A. Keren and J. S. Gardner, Phys. Rev. Lett. **87**, 177201 (2001).
- [2] P. Carretta, N. Papinutto, C. B. Azzoni, M. C. Mozzati, E. Pavarini, S. Gonthier, and P. Millet, Phys. Rev. B **66**, 094420 (2002).
- [3] F. Ye, Y. Ren, Q. Huang, J. A. Fernandez-Baca, P. Dai, J. W. Lynn, and T. Kimura, Phys. Rev. B **73**, 220404 (2006).
- [4] J. C. E. Rasch, M. Boehm, C. Ritter, H. Mutka, J. Schefer, L. Keller, G. M. Abramova, A. Cervellino, and J. F. Löffler, Phys. Rev. B **80**, 104431 (2009).
- [5] S. J. E. Carlsson, G. Rouse, I. Yamada, H. Kuriki, R. Takahashi, F. Lévy-Bertrand, G. Girit, and A. Gauzzi, Phys. Rev. B **84**, 094455 (2011).
- [6] K. Park, J. Oh, J. C. Leiner, J. Jeong, K. C. Rule, M. D. Le, and J.-G. Park, Phys. Rev. B **94**, 104421 (2016).
- [7] J. Oh, M. D. Le, H.-H. Nahm, H. Sim, J. Jeong, T. G. Perring, H. Woo, K. Nakajima, S. Ohira-Kawamura, Z. Yamani, Y. Yoshida, H. Eisaki, S. W. Cheong, A. L. Chernyshev, and J.-G. Park, Nature Communications **7**, 13146 (2016).
- [8] T. Kim, K. Park, J. C. Leiner, and J.-G. Park, Journal of the Physical Society of Japan **88**, 081003 (2019), <https://doi.org/10.7566/JPSJ.88.081003>.
- [9] D. Vaclavkova, A. Delhomme, C. Faugeras, M. Potemski, A. Bogucki, J. Suffczyński, P. Kossacki, A. R. Wildes, B. Grémaud, and A. Saúl, 2D Materials **7**, 035030 (2020).
- [10] A. McCreary, T. T. Mai, F. G. Utermohlen, J. R. Simpson, K. F. Garrity, X. Feng, D. Shcherbakov, Y. Zhu, J. Hu, D. Weber, K. Watanabe, T. Taniguchi, J. E. Goldberger, Z. Mao, C. N. Lau, Y. Lu, N. Trivedi, R. Valdés Aguilar, and A. R. Hight Walker, Nature Communications **11**, 2041 (2020).
- [11] Y. O. Kvashnin, A. Bergman, A. I. Lichtenstein, and M. I. Katsnelson, Phys. Rev. B **102**, 115162 (2020).
- [12] I. V. Solovyev, Phys. Rev. B **107**, 054442 (2023).
- [13] B. Sadhukhan, A. Bergman, Y. O. Kvashnin, J. Hellsvik, and A. Delin, Phys. Rev. B **105**, 104418 (2022).
- [14] M. Fechner, A. Sukhov, L. Chotorlishvili, C. Kenel, J. Berakdar, and N. A. Spaldin, Phys. Rev. Mater. **2**, 064401 (2018).
- [15] M. Först, R. I. Tobey, S. Wall, H. Bromberger, V. Khanna, A. L. Cavalieri, Y.-D. Chuang, W. S. Lee, R. Moore, W. F. Schlotter, J. J. Turner, O. Krupin, M. Trigo, H. Zheng, J. F. Mitchell, S. S. Dhesi, J. P. Hill, and A. Cavalleri, Phys. Rev. B **84**, 241104 (2011).
- [16] C. Dornes, Y. Acremann, M. Savoini, M. Kubli, M. J. Neugebauer, E. Abreu, L. Huber, G. Lantz, C. A. F. Vaz, H. Lemke, E. M. Bothschafter, M. Porer, V. Esposito, L. Rettig, M. Buzzi, A. Alberca, Y. W. Windsor, P. Beaud, U. Staub, D. Zhu, S. Song, J. M. Glowina, and S. L. Johnson, Nature **565**, 209 (2019).
- [17] S. R. Tauchert, M. Volkov, D. Ehberger, D. Kazenwadel, M. Evers, H. Lange, A. Donges, A. Book, W. Kreuzpaintner, U. Nowak, and P. Baum, Nature **602**, 73 (2022).
- [18] N. Ogawa, W. Koshibae, A. J. Beekmana, N. Nagaosa, M. Kubota, M. Kawasaki, and Y. Tokura, PNAS **112**, 8977–8981 (2015).
- [19] M. Xu, J. Puebla, F. Auvray, B. Rana, K. Kondou, and Y. Otani, Phys. Rev. B **97**, 180301 (2018).
- [20] X. Li, D. Labanowski, S. Salahuddin, and C. S. Lynch, Journal of Applied Physics **122**, 043904 (2017), <https://doi.org/10.1063/1.4996102>.
- [21] D. A. Garanin and E. M. Chudnovsky, Phys. Rev. B **92**, 024421 (2015).
- [22] S. Streib, N. Vidal-Silva, K. Shen, and G. E. W. Bauer, Phys. Rev. B **99**, 184442 (2019).
- [23] A. Rückriegel, S. Streib, G. E. W. Bauer, and R. A. Duine, Phys. Rev. B **101**, 104402 (2020).
- [24] J. H. Mentink, M. I. Katsnelson, and M. Lemieshko, Phys. Rev. B **99**, 064428 (2019).
- [25] M. Afmann and U. Nowak, Journal of Magnetism and Magnetic Materials **469**, 217 (2019).
- [26] P.-W. Ma, C. H. Woo, and S. L. Dudarev, Phys. Rev. B **78**, 024434 (2008).
- [27] D. Perera, M. Eisenbach, D. M. Nicholson, G. M. Stocks, and D. P. Landau, Phys. Rev. B **93**, 060402 (2016).
- [28] M. Strungaru, M. O. A. Ellis, S. Ruta, O. Chubykalo-Fesenko, R. F. L. Evans, and R. W. Chantrell, Phys. Rev. B **103**, 024429 (2021).
- [29] K. F. Garrity, Phys. Rev. B **99**, 174108 (2019).
- [30] J. Hellsvik, D. Thonig, K. Modin, D. Iuşan, A. Bergman, O. Eriksson, L. Bergqvist, and A. Delin, Phys. Rev. B **99**, 104302 (2019).
- [31] S. Mankovsky, S. Polesya, H. Lange, M. Weisshofer, U. Nowak, and H. Ebert, Phys. Rev. Lett. **129**, 067202 (2022).
- [32] H. Ebert, D. Ködderitzsch, and J. Minar, Rep. Prog. Phys. **74** (2011), 10.1088/0034-4885/74/9/096501.
- [33] E. N. Economou, K. L. Ngai, T. L. Reinecke, J. Ruvalds, and R. Silberglitt, Phys. Rev. B **13**, 3135 (1976).

- [34] S. J. Allen and H. J. Guggenheim, *Phys. Rev. B* **4**, 937 (1971).
- [35] J. B. Torrance and J. C. Slonczewski, *Phys. Rev. B* **5**, 4648 (1972).
- [36] S. Nikolov, M. A. Wood, A. Cangi, J.-B. Maillet, M.-C. Marinica, A. P. Thompson, M. P. Desjarlais, and J. Tranchida, *npj Computational Materials* **7**, 153 (2021).
- [37] J. W. D. Connolly and A. R. Williams, *Phys. Rev. B* **27**, 5169 (1983).
- [38] A. I. Liechtenstein, M. I. Katsnelson, V. P. Antropov, and V. A. Gubanov, *jmmm* **67**, 65 (1987).
- [39] L. Udvardi, L. Szunyogh, K. Palotás, and P. Weinberger, *Phys. Rev. B* **68**, 104436 (2003).
- [40] H. Ebert and S. Mankovsky, *Phys. Rev. B* **79**, 045209 (2009).
- [41] S. Mankovsky, S. Polesya, and H. Ebert, *Phys. Rev. B* **101**, 174401 (2020).
- [42] H. Ebert and S. Mankovsky, *Phys. Rev. B* **79**, 045209 (2009).
- [43] H. Ebert, J. Braun, D. Ködderitzsch, and S. Mankovsky, *Phys. Rev. B* **93**, 075145 (2016).
- [44] A. H. MacDonald and S. H. Vosko, *J. Phys. Chem.* **12**, 2977 (1979).
- [45] E. Engel and R. M. Dreizler, *Density Functional Theory – An advanced course* (Springer, Berlin, 2011).
- [46] M. E. Rose, *Relativistic Electron Theory* (Wiley, New York, 1961).
- [47] X. He, N. Helbig, M. J. Verstraete, and E. Bousquet, *Computer Physics Communications* **264**, 107938 (2021).
- [48] N. Stefanou, P. J. Braspenning, R. Zeller, and P. H. Dederichs, *Phys. Rev. B* **36**, 6372 (1987).
- [49] N. Papanikolaou, R. Zeller, P. H. Dederichs, and N. Stefanou, *Phys. Rev. B* **55**, 4157 (1997).
- [50] S. Mankovsky, H. Lange, S. Polesya, and H. Ebert, *arXiv* (2022), 10.48550/ARXIV.2212.12430.
- [51] T. Hühne and H. Ebert, *Phys. Rev. B* **65**, 205125 (2002).
- [52] M. Seemann, D. Ködderitzsch, S. Wimmer, and H. Ebert, *Phys. Rev. B* **92**, 155138 (2015).
- [53] G. Breit, *Phys. Rev.* **39**, 616 (1932).
- [54] S. Mankovsky, S. Polesya, and H. Ebert, *Phys. Rev. B* **101**, 174401 (2020).
- [55] N. Y. Schmidt, R. Mondal, A. Donges, J. Hintermayr, C. Luo, H. Ryll, F. Radu, L. Szunyogh, U. Nowak, and M. Albrecht, *Phys. Rev. B* **102**, 214436 (2020).
- [56] O. N. Mryasov, U. Nowak, K. Y. Guslienko, and R. W. Chantrell, *Europhysics Letters* **69**, 805 (2005).
- [57] H. Ebert, “The munich spr-kkp package,” .
- [58] F. Engelsman, G. Wiegers, F. Jelinek, and B. Van Laar, *Journal of Solid State Chemistry* **6**, 574 (1973).
- [59] S. J. E. Carlsson, G. Rousse, I. Yamada, H. Kuriki, R. Takahashi, F. Lévy-Bertrand, G. Giriat, and A. Gauzzi, *Phys. Rev. B* **84**, 094455 (2011).
- [60] T. Kimura, T. Goto, H. Shintani, K. Ishizaka, T. Arima, and Y. Tokura, *Nature* **426** (2003), 10.1038/nature02018.
- [61] K. Singh, A. Maignan, C. Martin, and C. Simon, *Chemistry of Materials* **22**, 5007 (2009).
- [62] S. Angelov and J. Doumerc, *Solid State Communications* **77**, 213 (1991).
- [63] C. Delmas, G. Le Flem, C. Fouassier, and P. Hagemmuller, *Journal of Physics and Chemistry of Solids* **39**, 55 (1978).
- [64] T. Hewston and B. Chamberland, *Journal of Physics and Chemistry of Solids* **48**, 97 (1987).
- [65] I. I. Mazin, *Phys. Rev. B* **75**, 094407 (2007).
- [66] A. V. Ushakov, D. A. Kukusta, A. N. Yaresko, and D. I. Khomskii, *Phys. Rev. B* **87**, 014418 (2013).
- [67] A. Rückriegel, P. Kopietz, D. A. Bozhko, A. A. Serga, and B. Hillebrands, *Phys. Rev. B* **89**, 184413 (2014).
- [68] T. Holstein and H. Primakoff, *Phys. Rev.* **58**, 1098 (1940).

APPENDIX

Appendix A: SLC for Next-Nearest Neighbors

In this section the results for the change of the diagonal and off-diagonal components of the exchange coupling tensor are presented for next-nearest neighbors j of atom i with $|\mathbf{r}_{ij}| = 1.0 a_{\text{lat}}$. In contrast to the nearest neighbors, the investigation of the next-nearest neighbors has the feature that they lie in the x , y or z directions and not in a diagonal direction. Hence, the dependence of the modification of $J_{ij}^{\alpha\beta}$ on the direction of the distance vector \mathbf{r}_{ij} w.r.t. the displacement can be accessed directly.

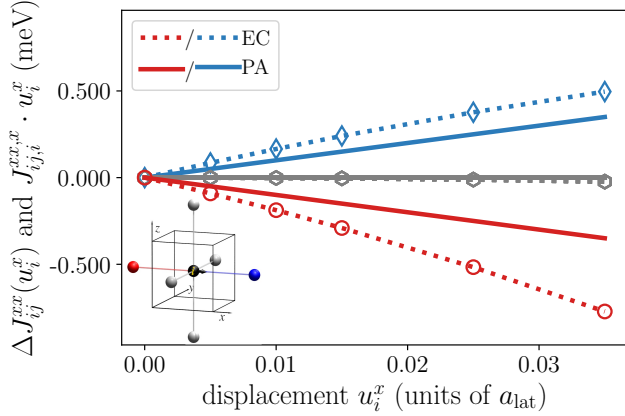


Figure 11. Modification of the diagonal exchange couplings of next-nearest neighbors for embedded clusters (EC) with 27 atoms (dotted lines) and the perturbative method (PA, solid lines) for a displacement in x direction in bcc Fe. The color-code of the atoms j is visualized in the inset figure: Red circles correspond to neighbors with $r_{ij}^x < 0$, blue diamonds to $r_{ij}^x > 0$ and grey hexagons to $r_{ij}^x = 0$.

In Tab. VII the results for the three-site SLC parameters calculated from 27 an 51 atomic clusters for a displacement of $0.005 a_{\text{lat}}$ in the x direction are compared to the perturbative approach. As for the nearest neighbors, the parameters for different cluster sizes agree within an accuracy up to the second digit. However, in contrast to the nearest neighbor case we find larger differences in the magnitudes of the embedded cluster and perturbative parameters. Nevertheless, the results agree quantitatively and show leading SLC contributions between the same next-nearest neighbors.

The isotropic part shown in Fig. 11 is mainly determined by the next-nearest neighbors j with $\mathbf{r}_{ij} \parallel \mathbf{u}_i$. In contrast, the off-diagonal contributions have the largest contributions from $\mathbf{r}_{ij} \perp \mathbf{u}_i$, e.g. for a displacement u_i^x in the perpendicular direction u_i^y . This can be seen

	27 atoms EC	51 atoms EC	PA
$(-1, 0, 0)$	-3.39	-3.36	-1.86
$(0, \pm 1, 0)$	-0.03	-0.03	0
$(0, 0, \pm 1)$	-0.03	-0.03	0
$(-1, 0, 0)$	3.159	3.12	1.86

neighbor	27 atoms EC	51 atoms EC	PA
$(-1, 0, 0)$	-0.09	-0.09	0
$(0, -1, 0)$	-0.28	-0.28	0.38
$(0, 0, \pm 1)$	0	0	0
$(0, -1, 0)$	0.28	0.28	0.38
$(-1, 0, 0)$	0.09	0.09	0

Table VII. Average absolute value of the off-diagonal SLC parameters $J_{ij,i}^{\text{diag},x} = \frac{1}{2} (J_{ij,i}^{xx,x} + J_{ij,i}^{yy,x})$ (top) and $J_{ij,i}^{\text{off},x} = \frac{1}{2} (J_{ij,i}^{xy,x} + J_{ij,i}^{yx,x})$ (bottom) in meV/a.u. for next-nearest neighbors, $i = k$ and a displacement in x direction in bcc Fe obtained by the embedded cluster (EC) method for clusters with 27 and 51 atoms and for the closed SLC expressions (averages over the values for the neighbors listed in each line). For the EC method $u_i^x = 0.005 a_{\text{lat}}$ was used.

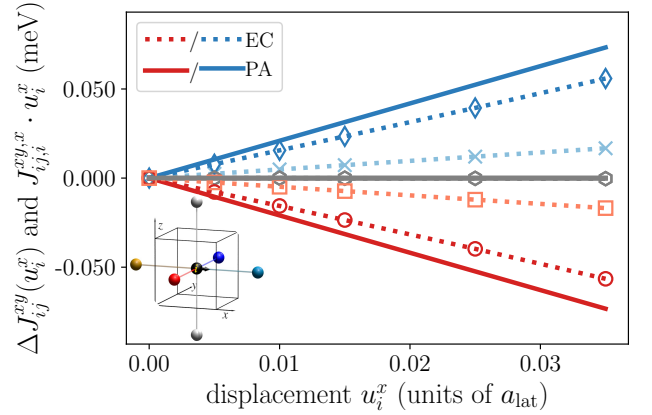


Figure 12. Modification of the off-diagonal exchange couplings of next-nearest neighbors for embedded clusters (EC) with 27 atoms (dotted lines) and the perturbative method (PA, solid lines) for a displacement of one atom in x direction for nearest neighbors in bcc Fe. The color-code of the atoms j is visualized in the inset figure: Dark red circles correspond to neighbors j with $\mathbf{r}_{ij} = (0, -1, 0)$, light red squares to $\mathbf{r}_{ij} = (-1, 0, 0)$, dark blue diamonds to $\mathbf{r}_{ij} = (0, 1, 0)$, light blue crosses to $\mathbf{r}_{ij} = (1, 0, 0)$ and grey hexagons to $r_{ij}^x = 0$.

in Fig. 12. Furthermore, one can already observe that $J_{ij,i}^{xy,x} \neq J_{ij,i}^{yx,x}$ (the latter is not shown here), which gives rise to an anti-symmetric (Dzyaloshinskii–Moriya) interaction already discussed in Ref. [31].

Appendix B: Fourier Transformed SLC

Following a similar procedure as e.g. proposed by Refs. [23, 31, 67] the magnetoelastic anisotropy energy due to DMI will be expressed in terms of spin creation and an-

annihilation operators. Introducing the spin lowering and raising operators into the DMI part of the SLC Hamiltonian Eq. (1) yields

$$\begin{aligned} H_{\text{SLC-DMI}} &= \frac{1}{S^2} \sum_{ij} \sum_{k,\mu} \left[D_{ij,k}^\mu (\hat{S}_i \times \hat{S}_j) \right] u_k^\mu \\ &= \frac{i}{2S^2} \sum_{ijk,\mu} \left[D_{ij,k}^{-\mu} (\hat{S}_i^z \hat{S}_j^+ - \hat{S}_i^+ \hat{S}_j^z) \right. \\ &\quad + D_{ij,k}^{+\mu} (\hat{S}_i^- \hat{S}_j^- - \hat{S}_i^- \hat{S}_j^+) \\ &\quad \left. + D_{ij,k}^{z\mu} (\hat{S}_i^+ \hat{S}_j^- - \hat{S}_i^- \hat{S}_j^+) \right] u_k^\mu, \end{aligned}$$

where the orientation vectors of the magnetic moments from the previous sections are replaced by normalized spin operators $\hat{S}_{i,j} \rightarrow \frac{1}{S} \hat{S}_{i,j}$. This can be rewritten in terms of creation and annihilation operators when using a Holstein-Primakoff transformation [68] to

$$\begin{aligned} H_{\text{SLC-DMI}} &= \frac{i}{S} \sum_{ijk,\mu} \left[D_{ij,k}^{-\mu} \sqrt{\frac{S}{2}} (\hat{b}_j - \hat{b}_i) \right. \\ &\quad + D_{ij,k}^{+\mu} \sqrt{\frac{S}{2}} (\hat{b}_i^\dagger - \hat{b}_j^\dagger) \\ &\quad \left. + D_{ij,k}^{z\mu} (\hat{b}_i \hat{b}_j^\dagger - \hat{b}_i^\dagger \hat{b}_j) \right] u_k^\mu. \end{aligned}$$

By applying a Fourier transformation for the bosonic creation and annihilation operators and lattice distortions one can define the Fourier transforms of the DMI components as follows:

$$D_{i,\mathbf{q}}^{x(y),\mu} = \sum_{\mathbf{R}_{ji}, \mathbf{R}_{ki}} D_{ij,k}^{x(y),\mu} e^{i\mathbf{q} \cdot \mathbf{R}_{ji}} e^{-i\mathbf{q} \cdot \mathbf{R}_{ki}} \quad (\text{B1})$$

and

$$D_{i,\mathbf{k}\mathbf{k}'}^{z,\mu} = \sum_{\mathbf{R}_{ik}, \mathbf{R}_{jk}} D_{ij,k}^{z,\mu} e^{-i\mathbf{k} \cdot \mathbf{R}_{ik}} e^{i\mathbf{k}' \cdot \mathbf{R}_{jk}}. \quad (\text{B2})$$

All together this results in

$$H_{\text{SLC-DMI}} = \frac{2i}{\sqrt{2S}} \sum_{\mu} \sum_{\mathbf{q}} \left[D_{\mathbf{q}}^{-\mu} \hat{b}_{\mathbf{q}} - D_{-\mathbf{q}}^{+\mu} \hat{b}_{-\mathbf{q}}^\dagger \right] u_{\mathbf{q}}^\mu \quad (\text{B3})$$

$$- \frac{2i}{\sqrt{NS}} \sum_{\mathbf{k}, \mathbf{k}'} \sum_{\mu} D_{\mathbf{k}, \mathbf{k}'}^{z\mu} \hat{b}_{\mathbf{k}}^\dagger \hat{b}_{\mathbf{k}'} u_{(\mathbf{k}' - \mathbf{k})}^\mu + \dots \quad (\text{B4})$$

As discussed by Refs. [22, 23, 67] the first two terms $D_{\mathbf{q}}^{-\mu} \hat{b}_{\mathbf{q}}$ ($D_{-\mathbf{q}}^{+\mu} \hat{b}_{-\mathbf{q}}^\dagger$) describe the interaction of a phonon and magnon, where a magnon is annihilated (created). The last term in Eq. (B4), $D_{\mathbf{k}, \mathbf{k}'}^{z\mu} \hat{b}_{\mathbf{k}}^\dagger \hat{b}_{\mathbf{k}'}$, represent the magnon-number conserving scattering processes since one magnon is annihilated and one is created [23]. Angular momentum can only be transferred between spins and lattice by magnon-number non-conserving processes (i.e. $D_{\mathbf{q}}^{-\mu} \hat{b}_{\mathbf{q}}$ and $D_{-\mathbf{q}}^{+\mu} \hat{b}_{-\mathbf{q}}^\dagger$).

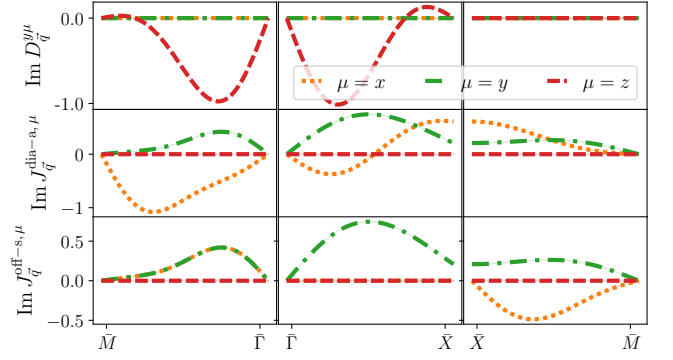


Figure 13. Imaginary part of SLC-DMI $\text{Im } D_{\mathbf{q}}^{x\mu}$ (top), anti-symmetric diagonal elements $\text{Im } J_{\mathbf{q}}^{\text{diag-a},\mu}$ (middle) and symmetric off-diagonal elements $\text{Im } J_{\mathbf{q}}^{\text{off-s},\mu}$ (bottom) of the SLC parameters in meV/a.u. for a Fe(001) monolayer, with $\mu = x, y, z$, plotted for \mathbf{q} along high-symmetry lines of the Brillouin zone. The real part is zero in all cases. Neighbors with $r_{ij} \leq 3.0 a_{\text{lat}}$ are considered.

To compare the SLC-DMI to other contributions of the SLC tensor a similar manipulation including the Fourier transformation of spin orientation vectors and displacements yields

$$H_{\text{SLC}} = \frac{1}{\sqrt{N}} \sum_{\mathbf{k}\mathbf{k}',\mathbf{q}} \sum_{\alpha\beta,\mu} J_{\mathbf{k},\mathbf{k}'}^{\alpha\beta,\mu} e_{\mathbf{k}}^\alpha e_{\mathbf{k}'}^\beta u_{\mathbf{q}}^\mu \delta_{\mathbf{k},\mathbf{k}'+\mathbf{q}} + \dots, \quad (\text{B5})$$

with

$$J_{i,\mathbf{k}\mathbf{k}'}^{\alpha\beta,\mu} = \sum_{\mathbf{R}_{ik}, \mathbf{R}_{jk}} J_{ij,k}^{\alpha\beta,\mu} e^{-i\mathbf{k} \cdot \mathbf{R}_{ik}} e^{i\mathbf{k}' \cdot \mathbf{R}_{jk}}. \quad (\text{B6})$$

Analogously, we find for the on-site parameters with $i = j$ that $\mathbf{k}' = 0$ in Eq. (B5) and

$$J_{i,\mathbf{q}}^{\alpha\beta,\mu} = \sum_{\mathbf{R}_{ik}} J_{ii,k}^{\alpha\beta,\mu} e^{-i\mathbf{q} \cdot \mathbf{R}_{ik}}. \quad (\text{B7})$$

In inversion symmetric crystals all contributions $D_{\mathbf{q}}^{\pm\mu}$, $D_{\mathbf{k},\mathbf{k}'}^{z\mu}$, $J_{\mathbf{k},\mathbf{k}'}^{\alpha\beta,\mu}$ and $J_{\mathbf{q}}^{\alpha\beta,\mu}$ are purely imaginary.

Appendix C: Connection to magnon and phonon dispersions

To investigate the impact of spin-lattice interactions on magnon and phonon modes the Fourier transformed spin-lattice contributions can be calculated (for further details see Ref. [31]). As an example, the results for Fe(001) are shown in Fig. 13. In the top panel the Fourier transformed SLC-DMI

$$D_{i,\mathbf{q}}^{x(y),\mu} = \sum_{\mathbf{R}_{ji}, \mathbf{R}_{ki}} D_{ij,k}^{x(y),\mu} e^{i\mathbf{q} \cdot \mathbf{R}_{ji}} e^{-i\mathbf{q} \cdot \mathbf{R}_{ki}}, \quad (\text{C1})$$

in the middle and bottom panels the Fourier transformed SLC related to on-site anisotropy

$$J_{i,\mathbf{q}}^{\alpha\beta,\mu} = \sum_{\mathbf{R}_{ik}} J_{ii,k}^{\alpha\beta,\mu} e^{-i\mathbf{q}\cdot\mathbf{R}_{ik}}. \quad (\text{C2})$$

are presented. These quantities represent the modification of magnon and phonon modes for a hybridization of these modes. For further details see Appendix B and Ref. [54]. Note that in contrast to the SLC presented in Tab. IV the Fourier transformations include the sum over neighboring atoms up to a distance of $3.0 a_{\text{lat}}$ to atom i and different configurations of the displaced atom. As discussed by Refs. [22, 23, 54, 67] the SLC-DMI $D_{\mathbf{q}}^{x(y)\mu}$ describe the interaction strength of a phonon and magnon, where a magnon is annihilated (created) and hence contribute to an angular momentum transfer. This is explained in further detail in Appendix B.

Appendix D: Splitting of the SLC according to exchange mechanism

Representing the isotropic exchange coupling parameters explicitly in terms of two contributions due to direct exchange (de) and superexchange (se), $J_{ij} = J_{ij}^{\text{de}} + J_{ij}^{\text{se}}$, one can see their impact also to different SLC parameters, assuming that J_{ij}^{de} depends on the distance $|\mathbf{R}_{ij}|$

and J_{ij}^{se} depends on the angle $\alpha(Cr_1 - O(S) - Cr_2)$. Variation of the distance by $u = \delta|\mathbf{R}_{ij}|$ results in the change of the direct contribution

$$J_{ij}^{\text{de}}(u) = J_{ij}^{\text{de},0} + \left. \frac{\partial J_{ij}^{\text{de}}}{\partial u} \right|_{u=0} u, \quad (\text{D1})$$

as well as the superexchange contribution (taking into account that the changes of the angle α due to displacement of Cr atom)

$$J_{ij}^{\text{se}}(\alpha + \Delta\alpha) = J_{ij}^{\text{se},0} + \left. \frac{\partial J_{ij}^{\text{se}}}{\partial \alpha} \right|_{u=0} \frac{\partial \alpha}{\partial u} u, \quad (\text{D2})$$

In the case of $\mathbf{R}_{ij} = (0, a, 0)$, the derivative $\frac{\partial}{\partial u} J_{ij}^{\text{de}}(u)$ is defined by the SLC parameter $\mathcal{J}_{ij,j}^{\text{se},y}$.

On the other hand, varying the distance $|\mathbf{R}_{ik}|$ with $k \neq i(j)$, e.g. along z direction, only the superexchange contribution gets a contribution linear w.r.t. the displacement $v_k^z = \delta R_{ik}^z$

$$J_{ij}^{\text{se}}(\alpha + \Delta\alpha) = J_{ij}^{\text{se}} + \left. \frac{\partial J_{ij}^{\text{se}}}{\partial \alpha} \right|_{u=0} \frac{\partial \alpha}{\partial v_k^z} v_k^z, \quad (\text{D3})$$

In this case the derivative $\frac{\partial}{\partial v_k^z} J_{ij}^{\text{se}}$ is defined by the SLC parameter $\mathcal{J}_{ij,k}^{\text{se},z}$.